A DESIGN TOOL FOR INERTIAL MICROFLUIDICS-BASED MICROCHIPS

EGE MUTLU

SEPTEMBER 2021

ÇANKAYA ÜNİVERSİTESİ

FEN BİLİMLERİ ENSTİTÜSÜ

MALZEME BİLİMİ VE MÜHENDİSLİĞİ
MİKRO VE NANOTEKNOLOJİ YÜKSEK LİSANS TEZİ

A DESIGN TOOL FOR INERTIAL MICROFLUIDICS-BASED MICROCHIPS

EGE MUTLU

SEPTEMBER 2021

ABSTRACT

A DESIGN TOOL FOR INERTIAL MICROFLUIDICS-BASED MICROCHIPS

MUTLU, Ege

M.Sc., Department of Materials Science and Engineering

Supervisor: Assoc. Prof. Dr. Ziya ESEN

Co-Supervisor: Assoc. Prof. Dr. Ender YILDIRIM

SEPTEMBER 2021, 64 pages

Microfluidic systems are frequently preferred for cell separation operations, which form the basis of the liquid biopsy concept. Cell separation processes can be done by applying different forces and taking advantage of different properties of cells. These are dielectrophoretic, magnetic, acoustophoretic, optophoretic and inertial forces. In order to take advantage of these forces and manipulate cells with the help of these forces, microfluidic channels must be designed with precision. Whether the designs work or not can be learned with experimental tests or with the help of numeric modeling programs. To test it experimentally, it is necessary to set up the microfluidic system and fabricate the microfluidic chip. This is an extremely time-consuming process. The importance of numeric modeling programs emerges here. By using numeric modeling programs, it is possible to test more than one design with different conditions and parameters without the need for microfluidic chip production. Although Numerical modeling programs are a very important alternative for microfluidic chip design, these programs have several limitations. First of all, these programs are programs that use high processer frequency, and a high-spec computer is needed for efficient modelling. This type of computer comes at a serious cost. In addition, these programs are programs with high prices in themselves. Having high prices makes these programs not easily accessible tools. Finally, and most importantly, using these

programs require serious software skills, theoretical background, and the ability to sense illogicality in results. In this study, a design tool for microfluidic chip with spiral shape microchannel. Microchips with the shape of spiral microchannels, take advantage of inertial forces to perform size-based cell separation, and it is widely used for cell separation applications. Unlike numerical modeling programs, this tool is aimed to be an easy-to-access, easy-to-use tool that can give feedback to users.

The design tool uses data from cell separation studies with spiral microfluidic channels to calculate the lateral positions of cells of different sizes in the user-designed spiral microchannel.

To be able to use the design tool, the user must have a few parameters and initial estimates for the targeted inter-cell distance. The tool calculates the distance between cells using parameter estimates and checks whether it meets the targeted distance. If the target is reached, the tool stops. but if the target is not reached, the tool will try higher flow values, find the required flow value to reach the target and give feedback to the user.

To see the efficiency of the design tool, spiral microchannels with different sizes, radius of curvatures was used, and channels were tested at 3 different flow rates. In the experiments, 2 different sizes of polystyrene microbeads were used to represent cells of different sizes. The reproducibility of the results obtained from the experiments was checked and the results were compared with the results obtained from the design tool. The comparisons revealed a ~10% difference between the experimental results and the results obtained from the design tool. Increasing the amount of data used by the design tool and changing the calculation methods used by the tool can be considered as a future work in order to give more accurate results.

Keywords: Microfluidics, liquid biopsy, cell separation, inertial microfluidics, spiral microchannel design, MEMS fabrication, microfluidic setup design

ÖZ

ATALETSEL MİKROAKIŞKAN ÇİPLER İÇİN BİR TASARIM ARACI

MUTLU, Ege
Yüksek Lisans, Malzeme Bilimi ve Mühendisliği
Tez Yöneticisi: Doç. Dr. Ziya ESEN
Yardımcı Tez Yöneticisi: Doç. Dr. Ender YILDIRIM
EYLÜL 2021, 64 sayfa

Sıvı biyopsi konseptinin temelini oluşturan hücre ayırma operasyonlarında mikroakışkan sistemler sıklıkla tercih edilmektedir. Hücre ayırma işlemleri, farklı kuvvetler uygulanarak ve hücrelerin farklı özelliklerinden yararlanılarak yapılabilir. Bunlar dielektroforetik, manyetik, akustik, optoforetik ve atalet kuvvetleridir. Bu kuvvetlerden yararlanmak ve bu kuvvetlerin yardımıyla hücreleri manipüle etmek için mikroakışkan kanalların hassas bir şekilde tasarlanması gerekir. Tasarımların çalışıp çalışmadığı deneysel testler veya sayısal modelleme programları yardımıyla öğrenilebilir. Deneysel olarak test etmek için mikroakışkan sistemi kurmak ve mikroakışkan çipi imal etmek gerekir. Bu son derece zaman alıcı bir süreçtir. Sayısal modelleme programlarının önemi burada ortaya çıkmaktadır. Sayısal modelleme programları kullanılarak mikroakışkan çip üretimine gerek kalmadan birden fazla tasarımı farklı koşul ve parametrelerle test etmek mümkündür. Sayısal modelleme programları mikroakışkan çip tasarımı için çok önemli bir alternatif olmasına rağmen, bu programların birkaç sınırlaması vardır. Öncelikle bu programlar yüksek işlemci frekansı kullanan programlardır ve verimli modelleme için yüksek özellikli bir bilgisayara ihtiyaç vardır. Bu tür bir bilgisayar ciddi bir maliyetle gelir. Ayrıca bu programlar kendi içinde fiyatları yüksek olan programlardır. Fiyatların yüksek olması bu programları kolay erişilebilir araçlar olmaktan çıkarıyor. Son olarak ve en önemlisi,

bu programları kullanmak ciddi yazılım becerileri, teorik altyapı ve sonuçlardaki mantıksızlığı sezme yeteneği gerektirir. Bu çalışmada, spiral şekilli mikrokanallı mikroakışkan çip için bir tasarım aracı. Spiral mikrokanal şeklindeki mikroçipler, boyuta dayalı hücre ayırma gerçekleştirmek için atalet kuvvetlerinden yararlanır ve hücre ayırma uygulamalarında yaygın olarak kullanılır. Bu aracın sayısal modelleme programlarından farklı olarak, kullanıcılara geri bildirim verebilen, erişimi kolay, kullanımı kolay bir araç olması hedeflenmiştir.

Tasarım aracı, kullanıcı tarafından tasarlanmış spiral mikrokanalda farklı boyutlardaki hücrelerin yanal konumlarını hesaplamak için spiral mikroakışkan kanallarla hücre ayırma çalışmalarından elde edilen verileri kullanır.

Tasarım aracını kullanabilmek için, kullanıcının hedeflenen hücreler arası mesafe için birkaç parametreye ve ilk tahminlere sahip olması gerekir. Araç, parametre tahminlerini kullanarak hücreler arasındaki mesafeyi hesaplar ve hedeflenen mesafeyi karşılayıp karşılamadığını kontrol eder. Hedefe ulaşılırsa araç durur. ancak hedefe ulaşılmazsa araç daha yüksek akış değerleri deneyecek, hedefe ulaşmak için gerekli akış değerini bulacak ve kullanıcıya geri bildirimde bulunacaktır.

Tasarım aracının etkinliğini görmek için farklı boyutlarda, eğrilik yarıçaplarında spiral mikro kanallar kullanılmış ve kanallar 3 farklı akış hızında test edilmiştir. Deneylerde, farklı boyutlardaki hücreleri temsil etmek için 2 farklı boyutta polistiren mikro boncuk kullanılmıştır. Deneylerden elde edilen sonuçların tekrarlanabilirliği kontrol edilmiş ve sonuçlar tasarım aracından elde edilen sonuçlarla karşılaştırılmıştır. Karşılaştırmalar, deneysel sonuçlar ile tasarım aracından elde edilen sonuçlar arasında ~%10'luk bir fark ortaya çıkardı. Tasarım aracının kullandığı veri miktarının arttırılması ve aracın kullandığı hesaplama yöntemlerinin değiştirilmesi daha doğru sonuçlar verebilmek için ileriye dönük bir çalışma olarak değerlendirilebilir.

Anahtar Kelimeler : Mikroakışkanlar, sıvı biyopsisi, hücre ayrımı, ataletsel mikroakışkanlar, spiral mikrokanal tasarımı, MEMS üretimi, mikroakışkan test düzeneği tasarı mı

ACKNOWLEDGEMENTS

First of all, my advisor Assoc. Prof. Dr. Ziya ESEN and my co-advisor Assoc. Prof. Dr. Ender YILDIRIM, who did not spare me their support and wisdom within the scope of my thesis studies. I am grateful to them for giving me the opportunity to work with them.

I would like to thank to Mikro Biyosistemler A.Ş. family, Özge ZORLU, Ebru ÖZGÜR, Begüm ŞEN DOĞAN, Taylan TÖRAL, Buket ŞAHİN, Alper DEMİR, Gizem KARAYALÇIN, Şebnem ŞAHİN, Emel Çiftçi, which I am proud to be in for providing resources and equipment to my work.

I would like to thank my friends, Birce Nil UZAY, Murat KOLAY, Ela TÜRKEL, Orhan ÇOLAK, Gülten AKIN ÇOLAK, who have given me great support during my thesis studies.

Finally, I would like to thank the most important people in the world for me, my mother, father, grandmother, and my dogs, who always supported me during the thesis study.

TABLE OF CONTENTS

LIST OF FIGURES

LIST OF TABLES

CHAPTER 1

INTRODUCTION

Microfluidics is the science of manipulation of microliter scale fluids inside of micrometer-scale channels. After the “There is Plenty of Room at the Bottom” speech of Richard Feynman[1], people realize the importance and the advantages of miniaturization.

The first appearance of microfluidics in technological devices was on a copier machine. To improve printing speed and quality, microfluidic valves were used. In 1980s, microfluidics researchers were working on microscale pumps, valves, and sensors. [2] However, in 1990 Andreas Manz published an article named “Miniaturized Total Chemical Analysis System: A Novel Concept for Chemical sensing” [3]. The article has presented the idea of the usage of microfluidic devices on biological and chemical analysis systems. With the article, microfluidic devices started to be seen in life sciences and analytical chemical reaction applications such as diagnostics, gas detection systems, drug delivery systems, drug toxicity, particle separation applications. The vast possibilities of microfluidics attract more researchers and scientists. Microfluidics technology is a potential tool for particle separation applications due to the weak force requirement, and small sample requirement compared to fluidic systems. Microfluidics is a powerful technology for medical diagnostics. In the microfluidics, forces that are not significant in macro flows may dominate the flow in microfluidic systems. And with the help of the forces created in the system, particles can be separated from each other based on their size, elasticity, magnetic or electrical properties. The application of separation of different particles can be applied on cancer diagnostics. By taking advantage of the size difference between cancer cells and blood cells, cancer cells can be separated from blood cells and collected which means the diagnosis of cancer

1.1. CANCER DIAGNOSTICS

In 2020, 10 million people died due to cancer. According to the statistics provided by WHO (World Health Organization), cancer ranked first or the second line on the cause of death list. In early-stage diagnosed cases, the survival rate is nearly three times higher than the late-stage diagnosed cases. Cancer can be diagnosed via imaging techniques, tissue biopsy, or liquid biopsy.

1.1.1. Imaging methods

The clinicians use six imaging method for the cancer diagnostics. These are optical imaging, single-photon emission computed tomography (SPECT), positron emission tomography (PET), magnetic resonance imaging (MRI), ultrasound (US), and computed tomography (CT) [4].

A tissue can either scatter the photons or it can absorb the photons which leads us to divide the imaging methods into two main titles: Scatter-based and absorption-based. The scatter-based optical imaging method is fast and has high resolution. However, in this method, only superficial tissues can be examined. The maximum thickness of the tissue that can be examined is 3 mm [4]. On the other hand, the absorption-based imaging method can examine thicker tissues with the help of mathematical models. Here, mathematical models are used to analyze reflected and non-reflective rays. The resolution provided by the absorption-based imaging method is lower than the scatter-based imaging method.

The CT scan uses iodine to apply x-ray beam to the patient. X-ray rays passing through the body are weakened. This amount of attenuation is measured with the help of a computer and an image is created. The iodine source and x-ray detector are rotated around the patient to create a 3D image.

Magnetic resonance imaging uses the nucleus of the hydrogen atom, that abundant in fat, on the other hand, water molecules abundant in the body. The nucleus of the hydrogen atom contains a single proton. The hydrogen proton can be compared to a magnet with poles and spinning around itself. These poles do not face a certain direction like north and south, they rotate on a random axis. The MRI scanner has a magnetic field strength ranging from 0.5 to 1.5 Tesla [4], and within this magnetic field, hydrogen atom protons in the body align along the axis of the MRI scanner and

form magnetic vectors. In addition to the creation of a magnetic field during MR imaging, radio waves are also created. These radio waves deflect magnetic vectors and cause hydrogen protons to resonate. By changing the frequency of the radio waves, different regions are made to resonate, thereby resonating the hydrogen atoms in the body in the form of slices. In addition to the creation of a magnetic field during MR imaging, radio waves are also created. These radio waves deflect magnetic vectors and cause hydrogen protons to resonate. By changing the frequency of the radio waves, different regions are made to resonate, thereby resonating the hydrogen atoms in the body in the form of slices. When the radio wave source is turned off, the magnetic vectors come to resting situation, creating a counter radio wave. The MRI device measures the intensity of this wave and creates a cross-sectional image [5].

SPECT imaging uses the radioactive metal technetium (TC), and it traces the radioactivity levels. When the technetium decays it produces gamma rays and the direction of the gamma rays is fully random. Since it is impossible to focus gamma rays to a particular direction, only the perpendicular rays can be detected by the SPECT which makes the SPECT method inefficient.

The positron, an anti-matter that have the same mass but opposite charge with the electrons, is emitted by atoms with a heavy nucleus. On PET scan, the body bombarded with the positrons and when a positron contacts with an electron, the electron which is the matter and the positron which is the antimatter annihilates each other. They produce photons with 511 keV [4]. This tremendous amount of energy detected by the detection crystals of the PET scan machine. Cancer tissues tend to contain higher amount of electron density which enables the PET scan to detect the difference between a healthy tissue and unhealthy tissue. However, a healthy tissue might contain high electron density due many reasons such as drugs. Also, the positrons cannot travel long distances before it is absorbed by the body, reducing the efficiency of the PET scan method.

In ultrasound imaging, the body is radiated by ultrasound waves. The sound wave hits to a tissue and the tissue reflects the wave. Reflected wave sensed by the probe and the tissue detected by the ultrasound machine. It is a very old technology, and it is hard access many parts of the body.

1.1.2. Tissue Biopsy

Tissue biopsy, or needle biopsy, is the most used method in the diagnosis of cancer. It is done by taking samples from abnormal cell populations detected by imaging methods or physical examination with the help of a needle. The sample taken with the help of a needle is only stained with immunologic dyes sensitive to cancer cells, and if the dye is seen in the sample taken, cancer diagnosis is made. This method is extremely painful for patients, and it is not possible to do it before the cancer tissue reaches a certain size.

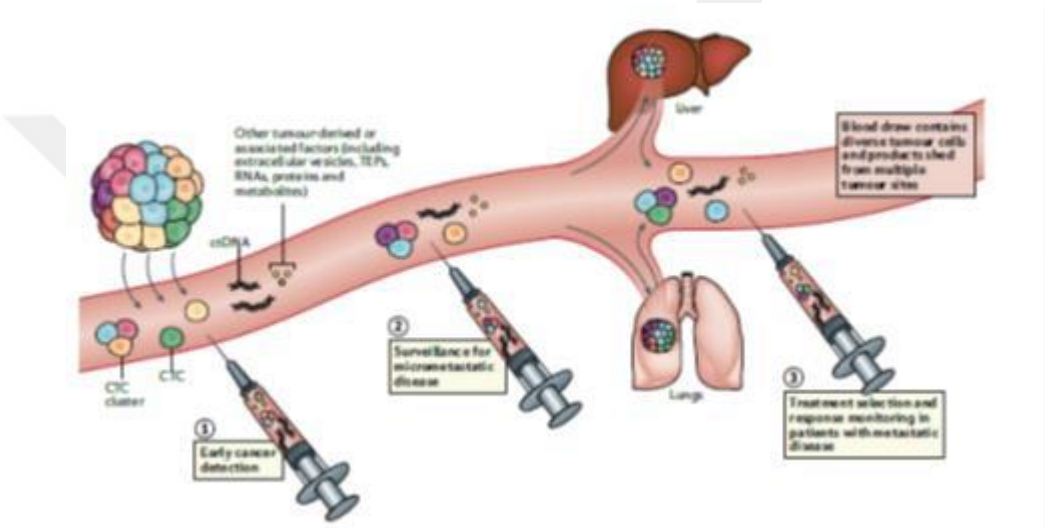

Figure 1 Metastasis phenomenon

1.1.3. Liquid Biopsy

Liquid biopsy can be defined as the diagnosis of the cancer by investigating the patients' blood for cancer materials such as tumor cells, tumor DNA, tumor mRNA, and exosomes. To understand the liquid biopsy concept, a phenomenon named metastasis should be investigated. Metastasis is responsible for 90 percent of cancer-related deaths [6]. Metastasis considered as the reason of the most deaths Metastasis phenomenon can be defined as the spread of cancer to the different organs or tissues from its original organ or tissue. A limited number of cancer cells can draw away from the cancer tissue and get into the bloodstream in cancer patients. These cells are named circulating tumor cells (CTCs). Circulating tumor cells circulating in the bloodstream can slip into another organ or tissue and cause the spread of cancer. Circulating tumor

cells are the main reason for metastasis, and it's hazardous for cancer patients. Liquid biopsy application aims to detect any cancer material that is circulating in the bloodstream. These materials are circulating tumor cells, circulating tumor DNAs, and exosomes. In this work, a design tool for the microfluidic chip that can be used to separate circulating tumor cells from white blood cells will be presented.

Liquid biopsy is a trendy topic among researchers and medical doctors recently. The reason behind this fact is pain-free and easy application, low cost of the liquid biopsy. However, the extreme rarity of the circulating tumor cells is the challenge fact of the liquid biopsy. A study among 70 patients with stage 3 and 4 non-small cell lung cancer showed that more than 5 CTCs were found in 7.5 ml of blood [7].

Liquid biopsy is considered as an alternative to tissue biopsy. However, it can substitute tissue biopsy with new scientific and engineering discoveries—comparison of the liquid and tissue biopsy given in the table 1.

Table 1 Comparison of tissue and liquid biopsy

	Tissue Biopsy	**Liquid Biopsy**
Technique	Taking sample via needle	Blood sample
Efficiency	High on the localized tumor tissue	Not very efficient with current technology
Availability of the disease monitoring	Not available	Real-time monitoring is available
Availability of the treatment monitoring	Not available without re-biopsy	Real-time monitoring is available
The pain inflicted on the patient	High	Low
Cost	High	Low
Required time	Moderate	Low

1.2. MICROFLUIDIC CELL SEPARATION TECHNIQUES

Particle separation can be done via active techniques such as dielectrophoresis (DEP), acoustophoresis, magnetophoresis (MAP), and optophoresis. Also, it can be done via passive techniques such as inertial microfluidics and filtration.

An external force is applied to the particles on active techniques, and the passive techniques, the force is generated by the microchannel geometry.

1.2.1. Dielectrophoresis (DEP)

A non-uniform electric field is generated via direct current or alternating current in dielectrophoresis. In the generated non-uniform electric field, the spatial gradient of the electric field and dipole of the cell interacts, and with that interaction, the particle starts to move.

To generate a non-uniform electric field, unique structures such as electrodes or insulated obstacles. Obtaining the non-uniform field via electrodes named as electro-based DEP and obtaining via insulators called insulator-based DEP. Ever since the world met the concept of CTC, it has been trying to separate CTC's from other blood cells and make different analyzes on them. For this purpose, tried to detect skin cancer cells in 1983 using the DEP method [8] . This is the first application of DEP in the field of liquid biopsy. DEP forces used to detect and separate many cancer types. [9] used DEP forces to detect HL-60 leukemia cells and [10] tried to detect MCF7 breast cancer cells. The challenge of the DEP is the changeable electrical specifications of the cells. Increment or decrement of the ions in a cell, changes its electrical property of the cell and since the DEP is taking advantage of the electrical properties of the cells, DEP forces change too. While designing the microfluidic chip and electrode network, it must be considered. Unavailability of applying high flow rate values and high dependency to the cell size are the further challenges of the DEP method [11].

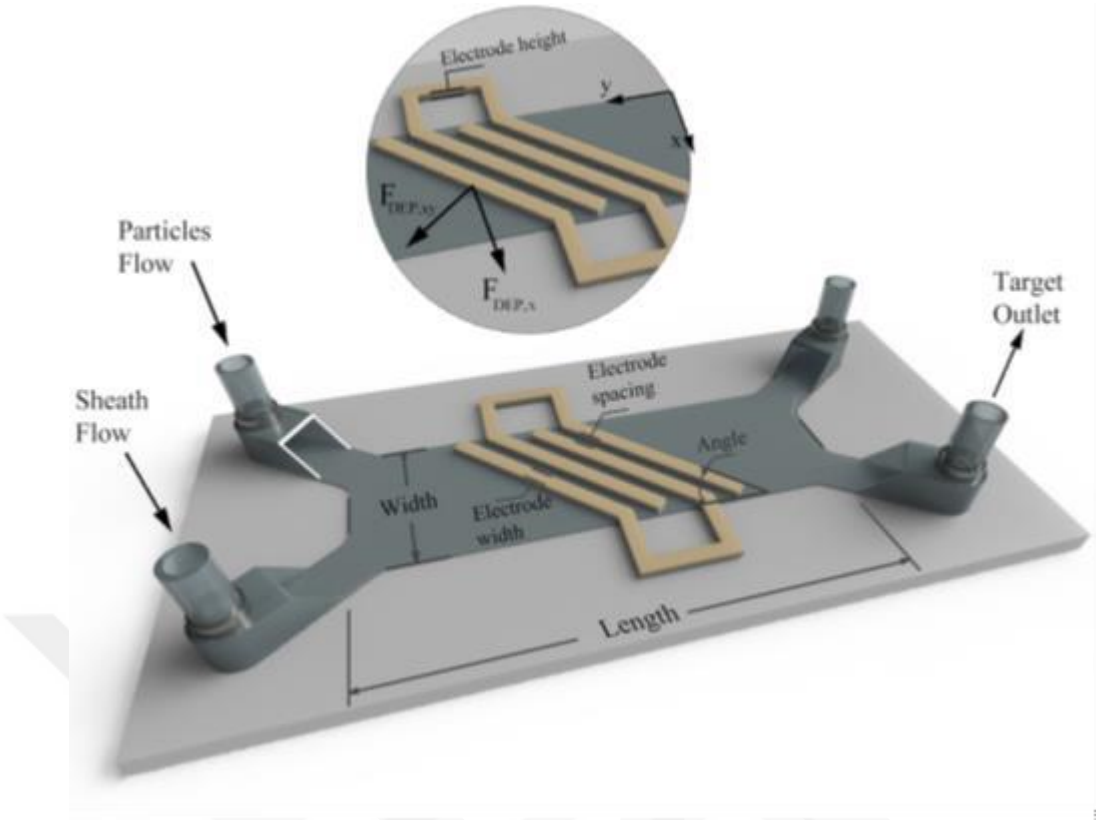

Figure 2 Example of a dielectrohoretic microchip

1.2.2. Acoustophoresis

Manipulation of the cells via ultrasonic radiation force is defined as acoustophoresis. Ultrasonic radiation forces are obtained via ultrasonic standing waves. Piezoelectric materials are used to generate ultrasonic waves in the microchannels.

Acoustophoresis is a trendy concept among microfluidic researchers. The reason behind this fact is the potential of acoustophoresis and unnecessity of labeling. Acoustophoresis is a relatively recent research topic then the other cell separation methods. Acoustophoretic devices were used for the separation of prostate [12], breast [13], cervical [13]and skin [14] cancer cells from blood cells. Among these applications of the acoustofluidic cell separation the applied flow rate varies between 20 µl/min and 100 µl/min which makes the operation takes too long relative to the hydrodynamic methods. In additional, piezoelectric materials are very fragile materials and for better acoustic radiation performance, the material of the microchip must be a brittle material. The brittle materials are relatively fragile compared to ductile materials. Due to this fact acoustophoretic microchips are fragile too.

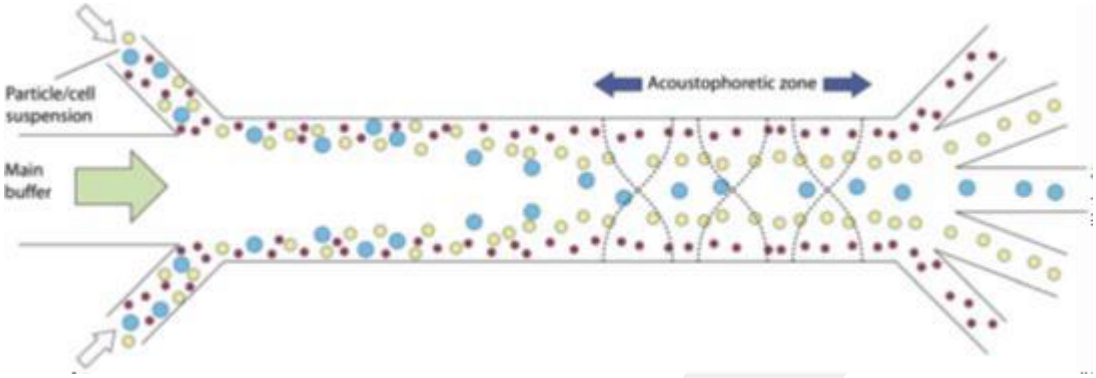

Figure 3 Acoustophretic cell separation

1.2.3. Magnetophoresis (MAP)

Magnetophoresis is cell manipulation via generated magnetic field. The main fact about magnetophoresis is to interact the cells or particles with the magnetic field. The particles that we are dealing need to be ferromagnetic to interact with the magnetic field. Unfortunately, cells and polystyrene microbeads are not ferromagnetic, and these materials have the leading role in cell separation application. Scientists and researchers solved that problem by coating these particles with ferromagnetic materials [15]. The magnetophoresis can be used to separate to the any type of cell that can be coated via ferromagnetic beads such as breast cancer cells [16], HeLa named cervical cancer cells [17] and non-small cell lung cancer cells [18]. Likewise, the magnetophoretic force can be used for cell isolation or cell manipulation. To trap a cell, the magnetophoretic forces must overcome the drag force generated due to the fluid flow. In this case, the applied flow rate must be lower than 1 mm/s [19]. On the other hand, cell manipulation operations have higher than 1mm/s flow rate limitations. Magnetic beads contain iron-based molecules such as Fe_2O_3 and Fe_3O_4 [20] which are very toxic for the cells. The toxicity reduces viability of the cell coated with magnetic beads which is a disadvantage of the magnetophoresis. Also, the inapplicability of the high flow rate values increases the operation time.

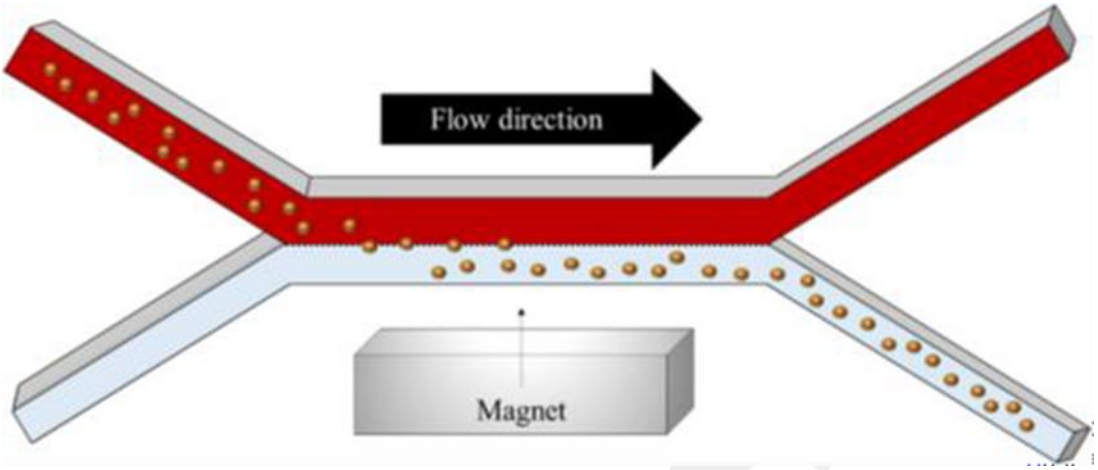

Figure 4 Magnetophoretic cell separation

1.2.4. Optophoresis

In the optophoresis method, an induced optical force is applied to the microfluidic channel, and due to the intrinsic specifications of the cells, the exerted force changes with the type of the particle. The optical force is generated by an optical tweezer. Optical tweezers are the devices that have focused laser beams. By taking advantage of the optical permeability specification of the cells, they can be separated. Optophoresis is generally used to separate metal particles, but it is used for cell trapping and cell manipulation in many studies. Yu et. al., tried to use optical methods to separate breast cancer, lung cancer, liver cancer, colon cancer and cervical cancer cells [21]. Because of using focused laser beams, the temperature inside of the microchannel increases. Also, there is a phenomenon called photodamage which is the damage done by the photons, reflected to the cells. Damaged cells could not be cultured and could not be used for down-stream analysis [22].

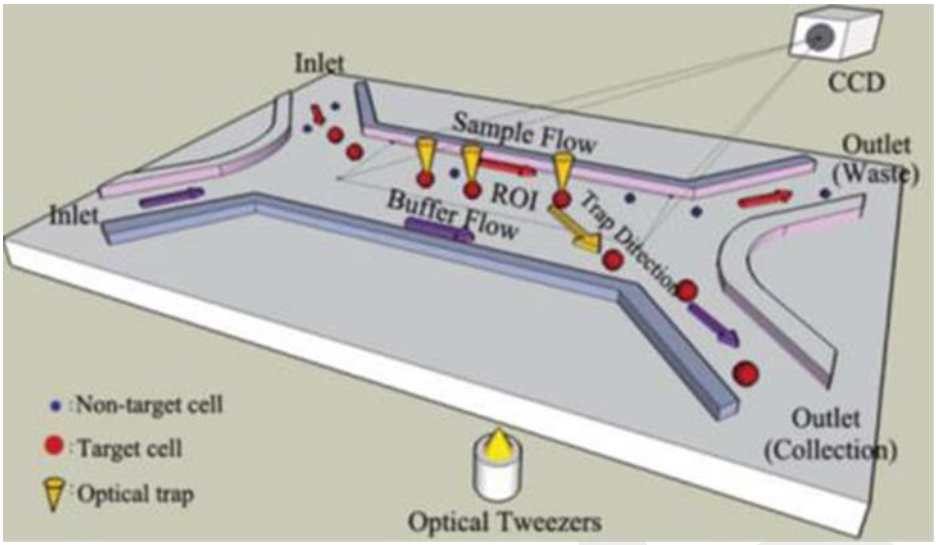

Figure 5 Example of an optophoretic microchip

1.2.5. Filtration

Filtration is a passive technique for cell separation. On the filtration technique, there are geometric structures with different gap lengths in the microchannel. The cells with large sizes cannot pass through the gaps between the geometries and are separated from the particles with smaller sizes.

Id et al. [23], presented a microfluidic chip for liquid biopsy applications. The microchip has a stair-like structure on the outlet ports which is permeable for the cells smaller than CTC's. Initial tests were done with human breast cancer cells.

The filtration technique works perfectly with rigid particles. However, some particles such as cells are not rigid. Cells can stretch between the smaller gaps than their sizes, reducing the efficiency of the separation.

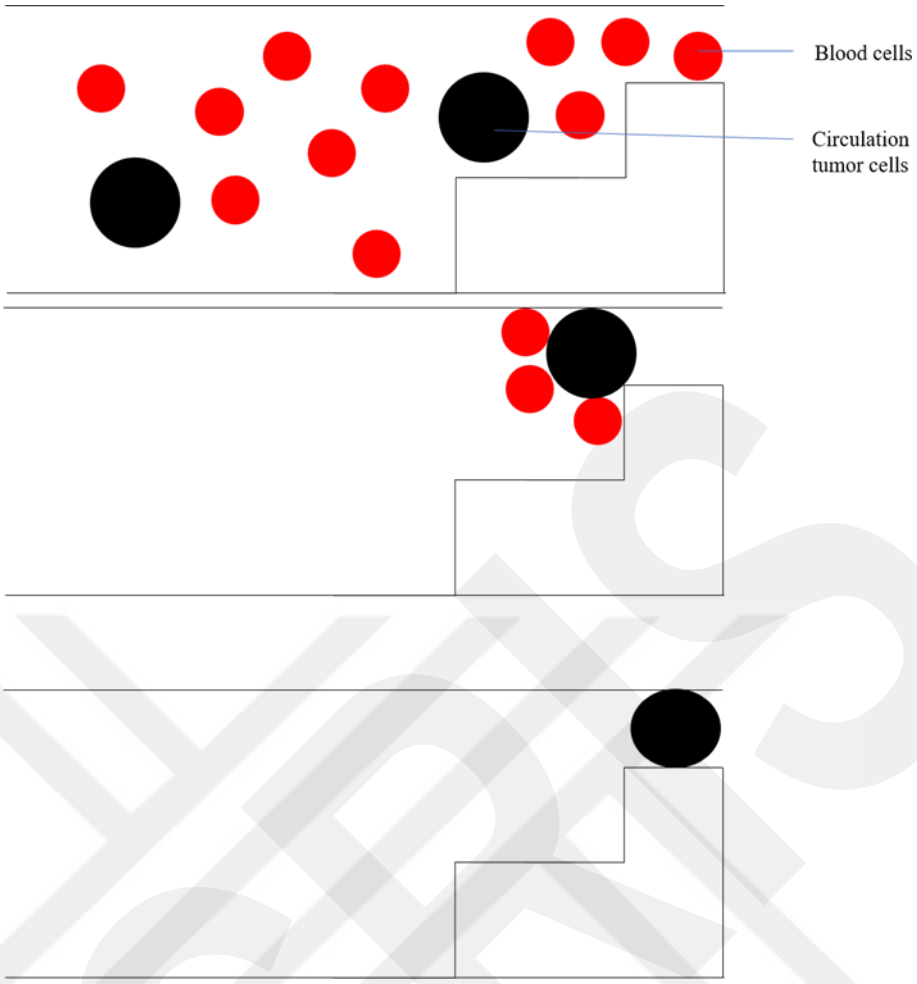

Figure 6 Mechanical filtration of cells

1.2.6. Inertial Microfluidics

The inertial microfluidics method is cell separation with the help of the forces created as a result of the resistance of the liquid and particles in the microchannel to movement. These forces occur in all microfluidic channels, but the flow in the channel must be high for them to have a noticeable effect. In a straight microchannel, only drag force and buoyancy force occur. These forces act on cells of different sizes in different sizes and enable them to reach a steady state at different points in the lateral direction in the channel. These steady positions are called focus points. In addition to these forces, there is another force called Dean force in curved channels, and this force enables the cells to come to the focusing points more quickly and provides an extension of the distance between the focusing points.

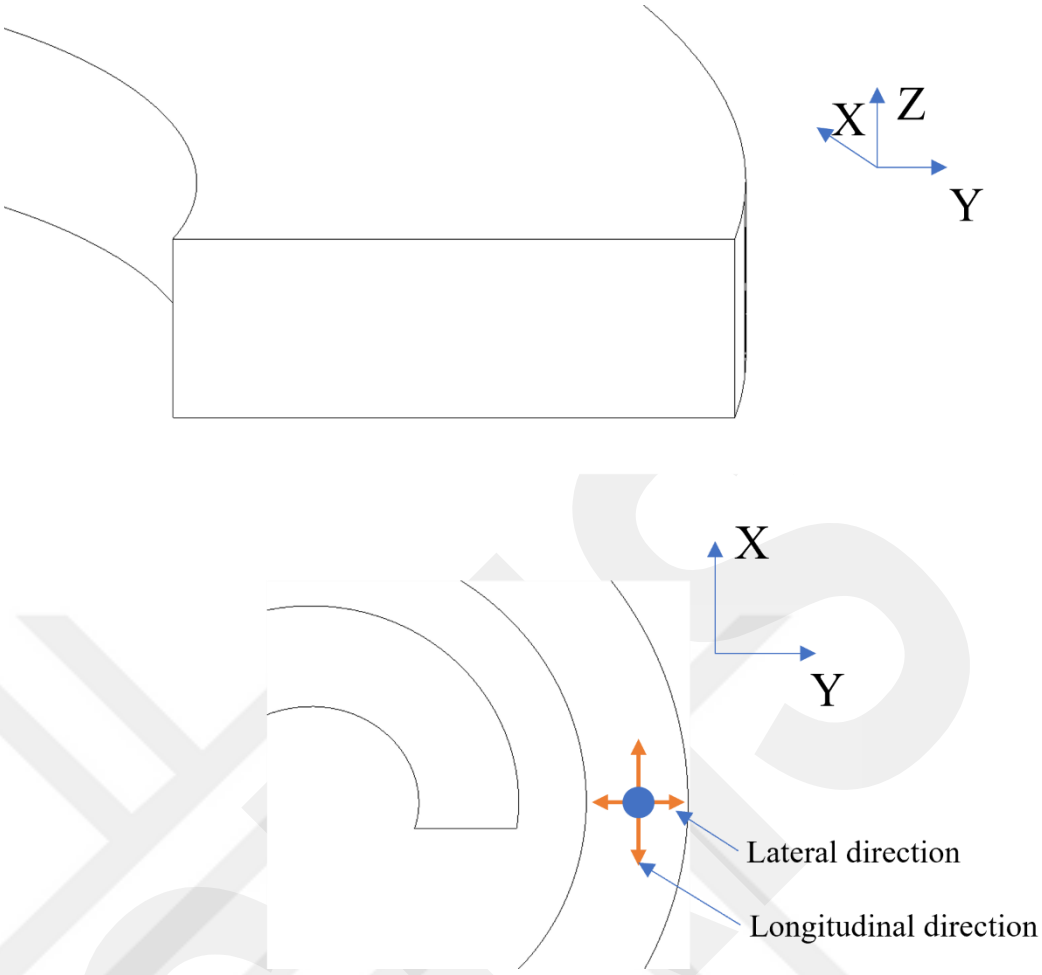

Figure 7 Lateral and longitudinal directions

Spiral-shaped and serpentine-shaped channels are examples of curved channels. In the design of these channels, there are main parameters that affect the cell separation efficiency. These are the channel dimensions, the radius of curvature, the dimensions of the cells to focus. The designer should make a precise design, considering these parameters and utilizing the principles of fluid mechanics.

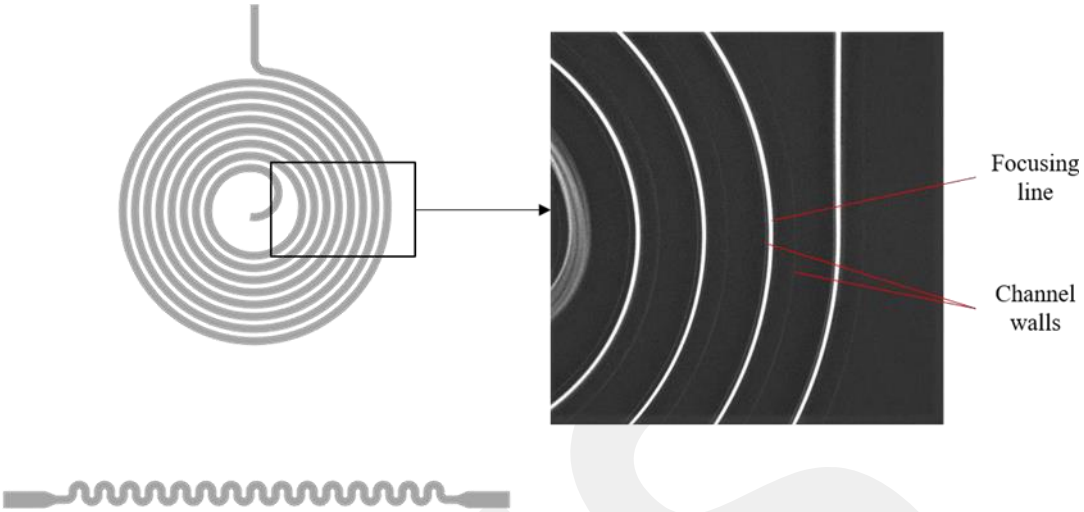

Figure 8 Spiral microchip and focused microbeads inside a spiral microchannel

1.3. OBJECTIVES

1.3.1. Problem Definition

The mission of the engineering is to solve any kind of problem that people faced with.

The microfluidic chip design is a process that combines ability of draw 3D objects, use of design software, fluid mechanics knowledge and engineering insight.

The steps of the microfluidic chip design given on the table below.

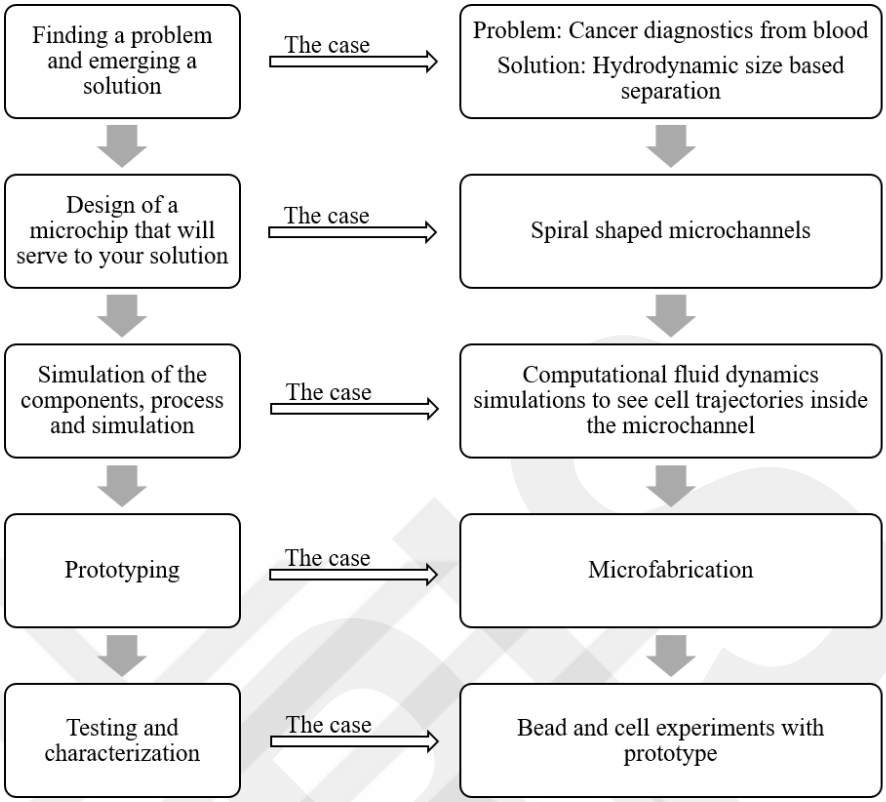

Figure 9 Design process of a Microfluidic device [24]

The thesis emerging a solution to the problems that are observed during simulation process. The simulations are done via help of the software called computational fluid dynamics (CFD). CFD software uses numerical approaches to solve the fluid mechanics problems. To do so, software divides the mechanical model to small pieces called meshes and solves equations for each mesh. The first problem cause for the CFD simulation is the mesh number. The number of mesh directly influences the solution on the CFD software. A simulation with a low mesh number can give inaccurate results. In contrast of high mesh number can increase the simulation time too much. Since the required time for simulation directly related with the performance of the computer, even the simulations with low mesh number can take unreasonable time with a low performance computer. Which is why the designer must conduct a mesh dependency study to find the optimum mesh number that is not affecting the results and not increasing the simulation time needlessly.

Within the scope of the thesis, CFD simulations were done to present the problem with exact numbers. The spiral microchannel with 200 um width and 80 um heights drawn

with Autodesk Fusion 360 software and imported to COMSOL Microfluidics CFD software.

The design process starts with defining a problem. The designer understands the problem and offers a solution the problem. In my case the problem is to diagnose cancer by body fluids.

- CFD problems for design
    - Low mesh number cause faulty results
    - High mesh number cause too much required time for simulation
    - Required time directly related with the performance of the computer
    - Simulations requires digital abilities
    - The designer must understand illogical results with fluid mechanics knowledge and experience

CHAPTER 2

THEORETICAL BACKGROUND

2.1. INERTIAL MICROFLUIDICS

Inertial microfluidics takes advantage of the inertial effects of the fluid flowing inside of the microchannel. On the generated flow environment, particle exerted several inertial forces these forces are viscous drag force, rotation induced lift force (Magnus force), slip shear-induced lift force (Saffman force), wall-induced lift force, shear gradient lift force, deformability-induced lift force, and dean force. These forces act on cells of different sizes in different sizes, and thus size-based separation can be made. After the particles moving in the channel are exposed to these forces for a certain distance, they get to the equilibrium position in the lateral axis and continue to move in this position [25].

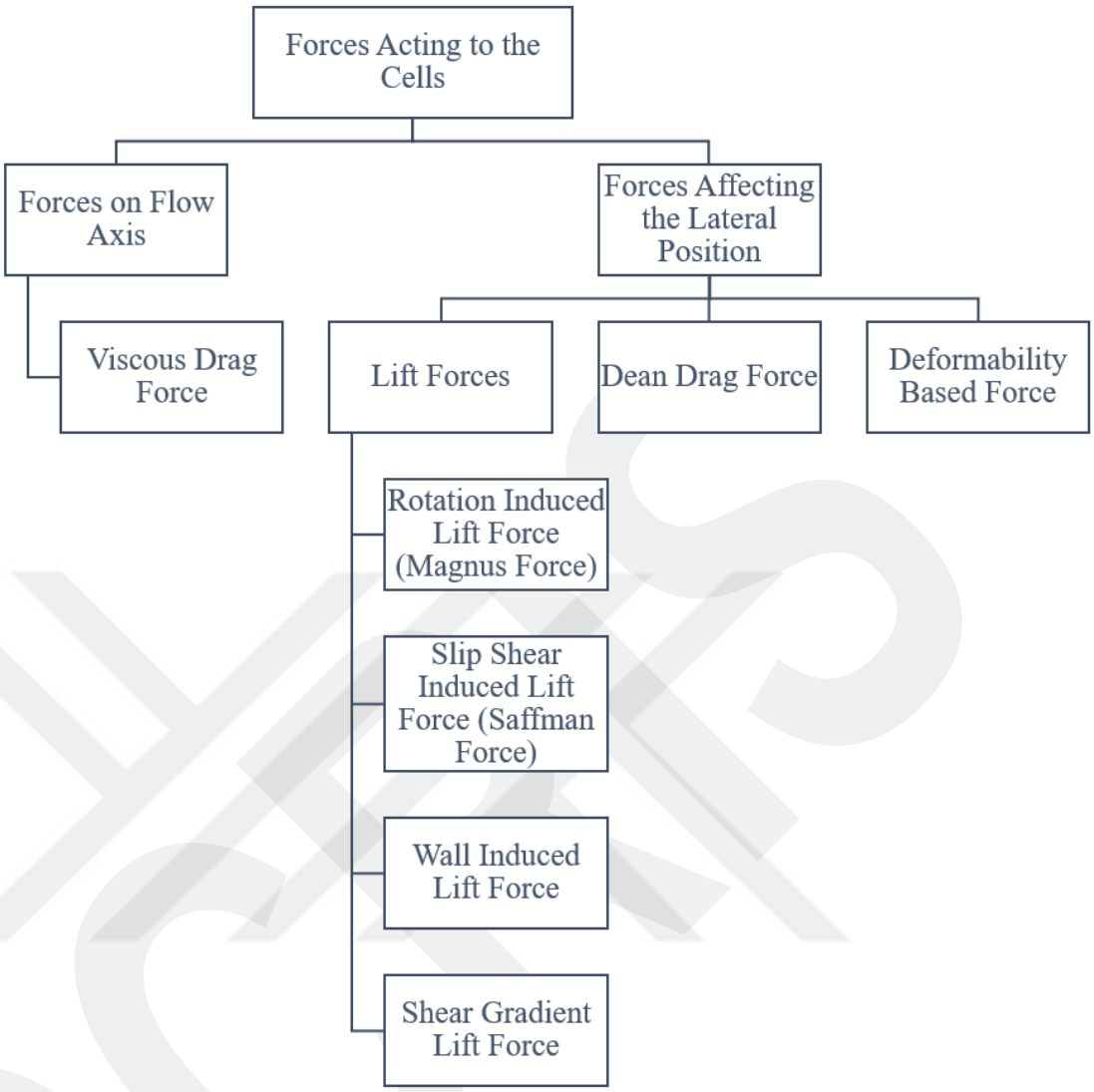

Figure 10 Forces acting on the cells on inertial microfluidics

Inertial effects manifest themselves in any channel with fluid flow, regardless of the geometric dimensions and shapes of the microchannels. These effects are due to the fluid flow itself. Inertial cell focusing can be applied in straight channels and curved channels. Owing to the secondary flow that occurs in curved channels, focusing cells in curved channels is easier and faster than focusing in straight channels. Spiral channels and serpentine channels are frequently used in inertial cell sorting applications.

2.2 INERTIAL FOCUSING

Inertial focusing takes place within any microchannel. It was observed that the lift forces acting on the cells began to focus the particles at certain points, and these focusing points were determined by the numerical computational fluid dynamics (CFD) method. In a circular microchannel, the particles are again focused on a circular shape. In the square and rectangular microchannels, the particles are focused as shown in figure 11.

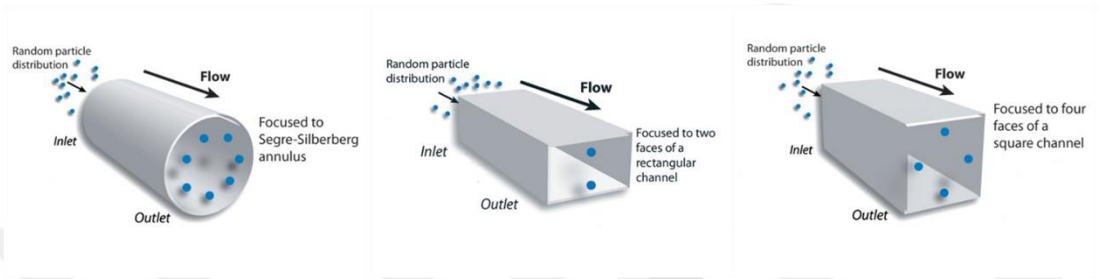

Figure 11 Expected focusing regions of the cell on different cross-section geometries [26]

Due to the difficulties of producing circular microchannels, square and rectangular microchannels are more frequently encountered. In this thesis, focusing of particles in microchannels with rectangular cross-section was investigated. Particles moving in rectangular cross-section microchannels are focused in two stages. In the first stage, the particles are focused as a line a certain amount above and below the centerline of the Z axis. In the second stage, the particles on this line come together and a point focus is formed as seen in figure 12.

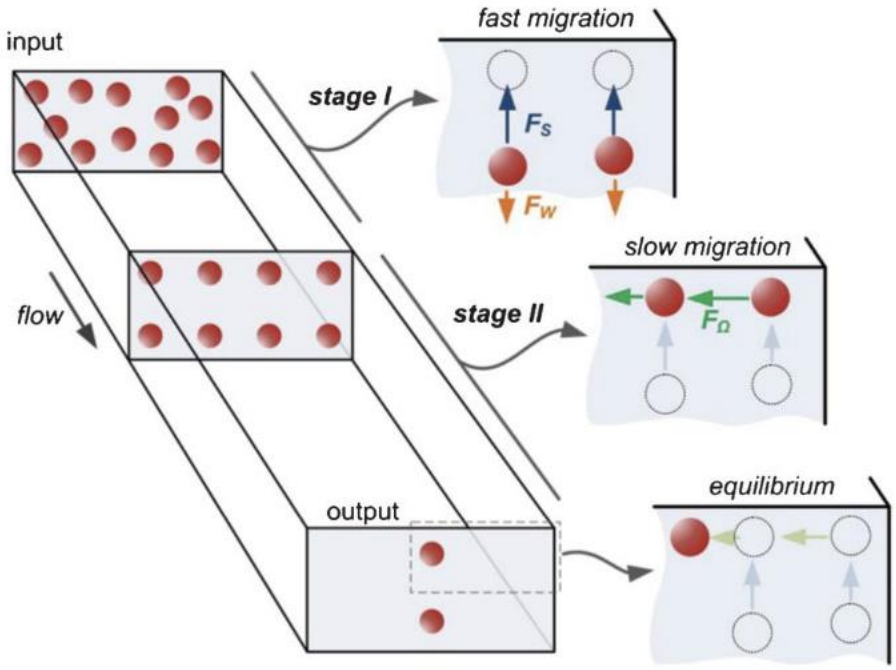

Figure 12 Focusing stage of the Inertial microfluidics [26]

2.2.1 Drag Force

Drag force is the force that occurred due to the velocity difference between the solid object, and fluid. Drag force is a resultant force of the interaction of fluid and solid particle; therefore, there are two musts to see drag force first must is the existence of a flow and a solid particle. The second must is the velocity difference between fluid and solid particles. The drag force is a longitudinal force that does not influence the lateral particle position. The direction of the drag force opposite to the direction of the flow as shown in the figure 13.

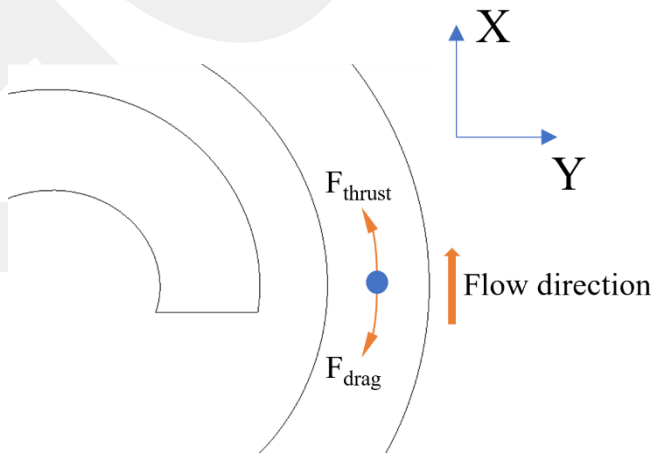

Figure 13 Direction the drag force

The formula of the drag force;

$$f_{drag} = (1.84Re'^{-0.31} + 0.293Re'^{0.06})^{3.45}\rho_f v_t^2 F_{drag}$$

$$= \frac{\pi}{4}a^2\rho_f U_t^2(1.84Re'^{-0.31} + 0.293Re'^{0.06})^{3.45}$$

$$Re = \frac{\rho U_{Max} D_H}{\mu}$$

$$D_H = \frac{2hw}{h+w}$$

Re: Reynolds Number

U_{Max}: Maximum velocity of the fluid

D_H: Hydraulic Diameter

ρ_f: Fluid Density

U_t: Relative velocity of fluid to particle

a: Particle diameter

2.2.2. Wall Induced Lift Force

Wall-induced lift force is the force generated due to the disturbance on the streamlines around the particle. The streamlines take position around the particle after it gets into the microchannel, and if the particle is too near to the microchannel wall, the streamlines become the way shown in the figure;

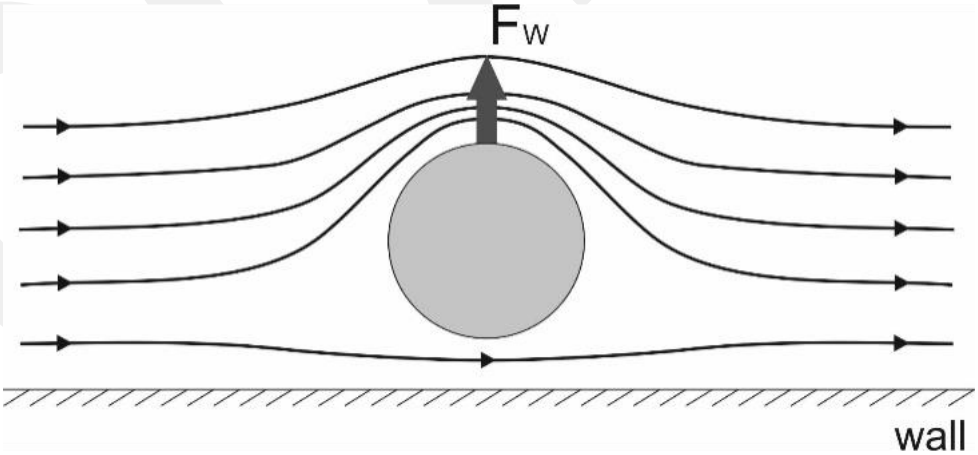

Figure 14 Wall induced lift force [26]

This type of disturbance on the streamlines causes pressure difference at the opposite sides of the particle, generating a force from the microchannel wall to the

center of the microchannel. This phenomenon is named wall-induced lift force (F_{LW})—the formulation of the Wall Induced Lift Force [27] given below.

$$F_{LW} = C_W \rho U_m^2 a_p^6 / D_h^4$$

C_W: Wall induced lift coefficient

U_m: Maximum flow velocity

D_h: Hydraulic diameter

2.2.3. Shear Induced Lift Force

The flow profile in the microchannel is non-linear due to the frictional force on the microchannel walls. Friction on the channel walls reduces the flow rate, and near the wall the flow almost stops. This causes the flow profile to take a parabolic shape as shown in the figure. This phenomenon is known in the literature as the Hagen-Poiseulle law.

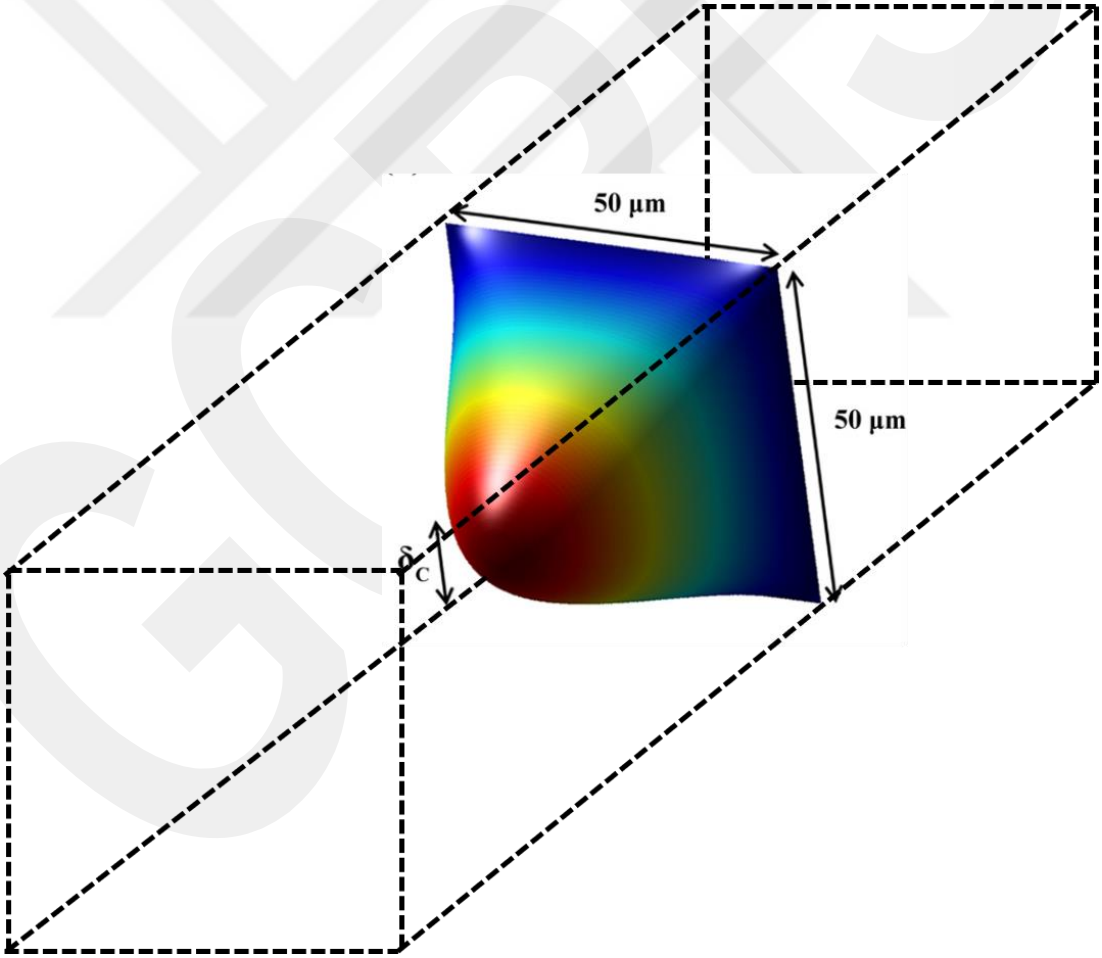

Figure 15 Velocity profile on Poiseuille flow [28]

Due to the velocity difference near the microchannel walls and the center of the microchannel, an imbalance in the pressure occurred. Shear-induced lift force is a consequence of this pressure imbalance. The direction of the force is from the center of the microchannel to the microchannel walls, which is the opposite of the wall-induced lift force as shown in the figure 16.

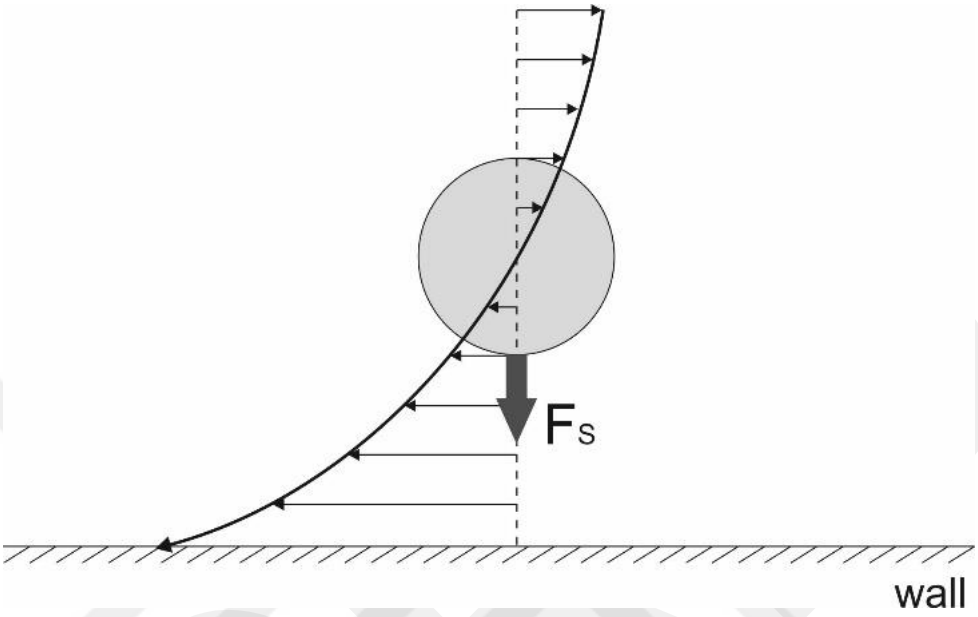

Figure 16 Shear induced lift force [26]

It is the most dominant force generated due to the geometry of the microchannels and the inertial effects of the fluids. The formula of the shear-induced lift force is;

$$F_S = C_S \rho U_m^2 a_p^3 / D_h$$

C_S: Shear induced lift coefficient

U_m: Maximum flow velocity

D_h: Hydraulic diameter

2.2.4. Rotation Induced Lift Force (Magnus force)

Under fully developed flow, the fluid velocity at the bottom of a spherical solid is different from the velocity at its top as a consequence of the rotational movement on its axis. As Bernoulli's principal yields, the difference in velocity means the difference in the pressure. The difference in the pressure on opposite sides generates a force (F_{LR}) that pulls the cell against channel wall.

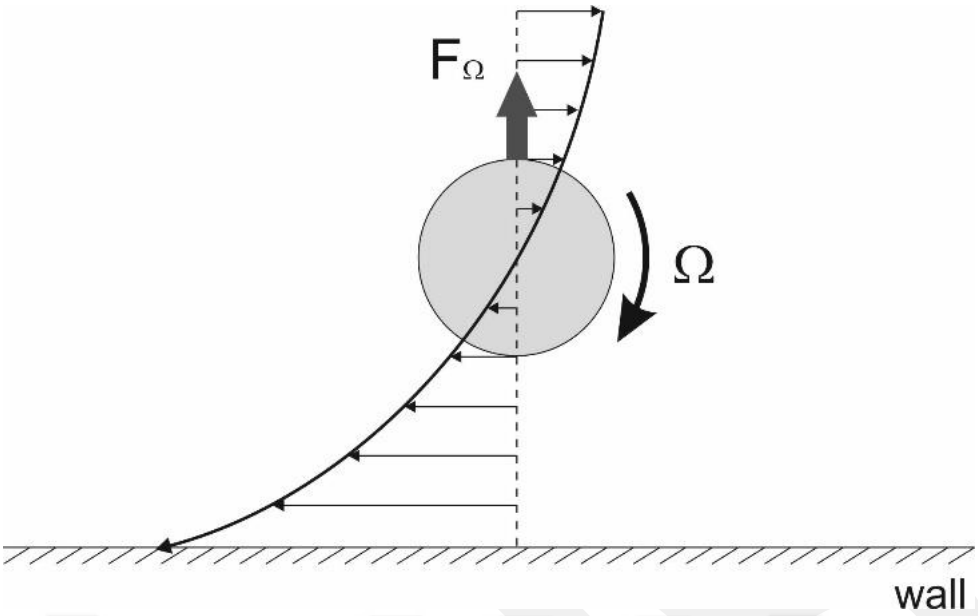

Figure 17 Rotation induced lift force [26]

The formula of the magnus force is:

$$\vec{F}_{LR} = \frac{1}{8}\pi a^3 \rho_f \vec{U} \times \vec{\Omega}$$

$\vec{U}$: Relative velocity

$\vec{\Omega}$: Contant angular velocity

2.2.5. Slip Shear Induced Lift Force (Saffman Force)

Slip shear force was discovered by P.G. Saffman in 1965. It is a force generated by the interaction of the velocity gradient of the fluid and the Stokes velocity field of the particle. The formula of the force is;

$$F_S = \frac{K}{4} U a^2 (\gamma v^{-1})^{1/2}$$

K: Numerical constant (K~81.2)

γ: Velocity gradient

υ: Kinematic viscosity

Saffman and Magnus forces are minimal compared with the wall induced and the shear induced lift forces, which is why they are generally neglected in the calculations.

2.2.6. Net Inertial Lift Force

In the light of this information, the net lift force can be defined within the micro-channel. The direction of the net lift force is from the center of the microchannel to the channel walls. Formulation of the lift force[27] is;

$$F_L = C_L \rho U_m^2 a_p^3 / D_h$$

C_L: Shear induced lift coefficient

U_m: Maximum flow velocity

D_h: Hydraulic diameter

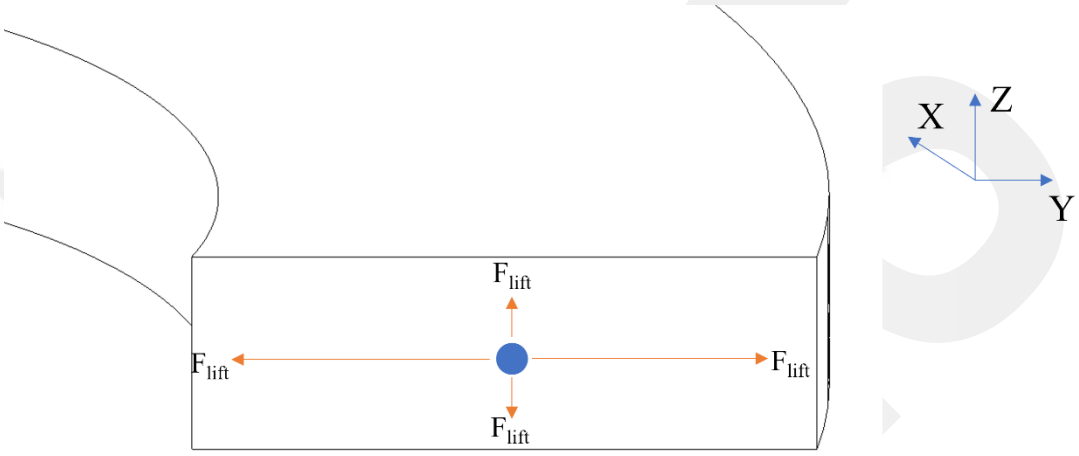

Figure 18 Direction of the lift force on the cross-section of the microchannel

Because of these forces, particles focus on specific points inside of the microchannel. The focusing points are changeable with the cross-sectional geometry of the channels. The figure below presents the positions expected as the particles' focusing points in different geometries.

2.2.7. Dean Flow and Dean Force

In a curved microchannel, due to the centripetal and centrifugal forces, an imbalance occurs on the velocity field inside of the microchannel. The velocity at the concave side is lower than the velocity at the convex side of the microchannel, as shown in the figure [29].

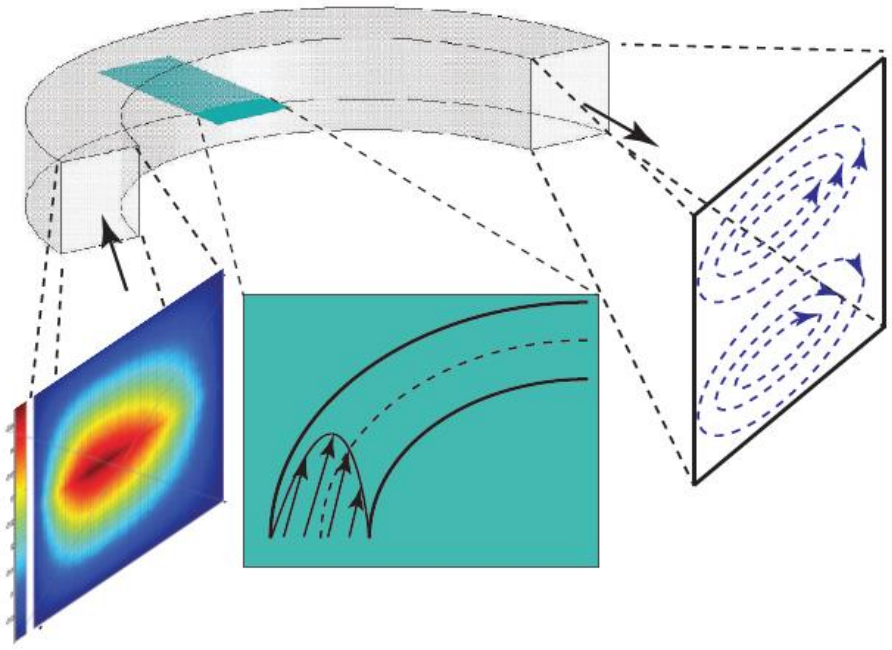

Figure 19 Velocity profile inside of a curved microchannel [28]

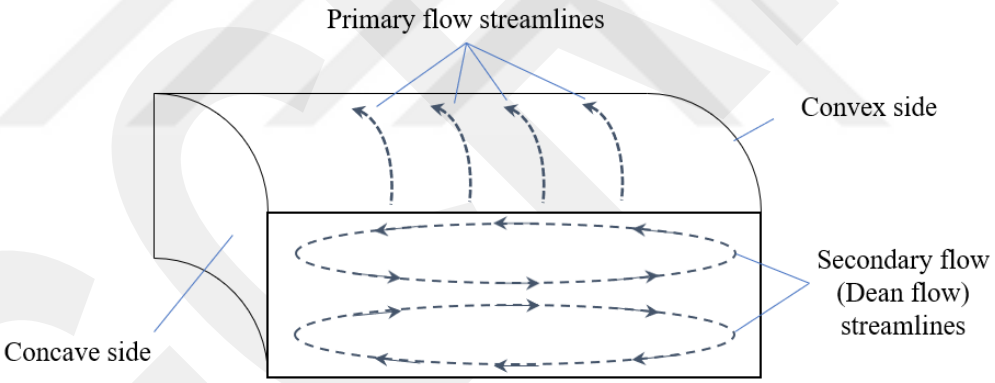

Figure 20 Secondary flow streamlines inside of a curved microchannel [29]

Centripetal force can be defined as the force required to move a particle in a curved channel. The direction of the force is from the concave side to the convex side. Oppositely the direction of the centrifugal force is from the convex side to the concave side, and it can be defined as the force pulling the particle towards the outer microchannel wall originated from the principle of inertia—the directions of the forces presented in the figure below.

The non-uniformity on the velocity generates a lateral secondary flow inside of the microchannel. W.R. Dean discovered this phenomenon, and it is named Dean Flow. The secondary flow divides the microchannel cross-section into two parts, the upper and lower parts. At the centerline of the microchannel, the direction of the streamlines is from the convex side to the concave side of the microchannel; afterward, the streamlines tend towards the center line to the microchannel wall. At the top and the bottom of the microchannel, the direction of the streamlines is the opposite of the streamline direction at the center of the channel. The path of the streamlines has a circle shape, and the physical equivalent of the circle-shaped streamline is a vortex. Vortices are the consequence of the secondary (Dean) flow. On the low Reynolds number flows, generally, two vortices are generated. On the other hand, number of vortices might be increased on the high Reynolds number flows. The Dean vortices are shown in the figure below.

W. R. Dean formulated the force acting on the particles due to the secondary flow. The formulas were obtained from experimental data. The formula contains concepts that have been discovered by W. R. Dean, such as Dean velocity and Dean number. These concepts are required for the formulation of the experimental data. The formula;

$$De = Re\sqrt{\frac{D_h}{2R}}$$

De: Dean number

R: Radius of curvature

Sorting cells with inertial microfluidics is one of the fast and efficient methods in the literature. With this motivation, different geometries are used. Di Carlo et.al. [30] size-based separation applications were made with the help of microchannels on the serpentine, which has an S shape. Cell separation with the aid of spiral microchannels is one of the most common inertial microfluidic applications. Different types of spirals have been used for this purpose. Warkiani et. al. [31], published size-based cell sorting using Archimedean spiral. Likewise, Mutlu et. al. [32] conducted studies on the separation of breast cancer cells from white blood cells by using Archimedean spiral and airfoil-like structures placed in the microchannel.

CHAPTER 3

DESIGN TOOL

3.1. WHAT IS THE DESIGN TOOL?

The design tool is a Microsoft excel-based tool designed to calculate the positions of particles of different sizes in spiral microchannels under different operational conditions. The design tool takes the design parameters specified by the users as input. These parameters are the width and height of the spiral microchannel, the dimensions of the cells where the spiral is planned to focus on the radius of the curvature of the canal, and the operational volumetric flow rate. Using this data, the design tool calculates the physical parameters within the channel that affect the focusing. Calculated parameters are given below.

Table 2 Important parameters for the inertial microfluidic cell focusing

Name of the parameter	Equation
Reynolds number (Re_C)	$\frac{\rho U_{Max} D_H}{\mu}$
Hydraulic diameter (D_H)	$\frac{2hw}{h+w}$
Confinement ratio (λ)	$\frac{a}{D_H}$
Radius of curvature ratio (δ)	$\frac{D_H}{2R}$
Dean number (De)	$Re_C \delta^{\frac{1}{2}}$

- ρ: Fluid density
- U_{Max}: Maximum velocity of the fluid ($\frac{3}{2}\,U_{Avg}$)
- μ: Fluid viscosity
- h: Height of the microchannel
- w: Width of the microchannel
- a: Particle size
- R: Radius of curvature

The Reynolds number (Re) is the ratio of the inertial forces to the viscosity forces of a fluid. The Reynolds number is used to denote different flow regimes such as laminar flow and turbulent flow.

Hydraulic diameter is a term used for making the analogy between circular cross section channels and non-circular microchannels. Most of the equations in microfluidics are valid for circular microchannels which is why we are calculating the hydraulic diameter of a non-circular microchannels, and we are using that measurement in our calculations.

Confinement ratio expresses the ratio of the size of the particles in the channel to the size of the channel. It is also used to predict whether a particle can or cannot be focused within the channel. Di Carlo's [27] work states that particles with a confinement ratio less than 0.07 cannot be focused in the microchannel with the help of hydrodynamic or inertial forces.

Radius of curvature ratio is equal to half the ratio of hydraulic diameter and radius of curvature. It is the parameter used to standardize spiral microchannels [33].

Dean number is a parameter used to calculate the magnitude of the secondary flow that occurs within curved microchannels. The Dean number was discovered by the English physicist W.R. Dean.

3.2. WHAT DOES THE TOOL OFFERS?

The tool offers an alternative to the simulation step of the design process. The design tool significantly shortens the simulation process, and besides shortening the process, it also eliminates the need for a high-performance computer. It calculates the focusing points of the cells that the design tool aims to focus on in the specific spiral channel of the users in approximately 2 seconds.

3.3. HOW DOES IT CALCULATES FOCUSING POSITIONS?

3.3.1. Calculation step

In the calculation step, the tool takes input parameters from the user which are named as the “Initial guesses” in the tool. The users chose the parameters by their facility and fabrication capabilities. These parameters are;

Table 3 Initial guesses to be filled by user

Initial Guesses	Example value
Channel width (um)	250
Channel height (um)	80
Radius of curvature (mm)	5
Size of the Particle 1 (um)	10
Size of the Particle 2 (um)	16
Volumetric flow rate (ml/min)	1.2

By using these parameters, tool calculates the following parameters which have critical role in inertial microfluidics.

Table 4 Critical parameters that is going to be calculated by tool

Critical parameters	Example value
Hydraulic diameter (um^2)	121.2
Confinement ratio of the particle 1	0.083
Confinement ratio of the particle 2	0.132
Radius of Curvature Ratio	0.0121
Average fluid velocity (m/s)	1.0
Maximum fluid velocity (m/s)	1.5
Average Reynolds number	121.2
Maximum Reynolds number	181.8
Dean Number	13.3

3.3.2. Conditions

Inertial microfluidics is a passive method for cell sorting and since there is no external force exerted on the cells, the fluid regime and inertial effect should satisfy for a sufficient cell sorting. This situation generates conditions for the critical parameters. The tool checks the values of the critical parameters and give feedback to the user if they are satisfying or not. Tool marks the cells green with satisfying parameters and marks the cells with red if the parameter is not satisfying.

The first is the value of confinement ratio of any particle that is aimed to separate from each other must be greater than 0.07 [27]. Second is the value of Dean number value must be greater than 10 and lesser than 25. The dean number must be greater than 10 because under that value the Dean force is not very effective with a

dean number value lesser than 10. Oppositely, the Dean force is over effective with a dean number value greater than 25[29].

Table 5 Green marked critical parameters

Calculated Parameter	
Hydraulic Diameter (µm^2)	121.2
Confinement Ratio of the Particle 1	0.083
Confinement Ratio of the Particle 2	0.132
Radius Of Curvature Ratio	0.0121
Average Fluid Velocity (m/s)	1.0
Maximum Fluid Velocity (m/s)	1.5
Reynolds Number	121.2
Maximum Reynolds Number	181.8
Dean Number	13.3

Table 6 Green and red marked critical parameters

Calculated Parameter	
Hydraulic Diameter (µm^2)	121.212
Confinement Ratio of the Particle 1	0.083
Confinement Ratio of the Particle 2	0.132
Radius Of Curvature Ratio	0.0121
Average Fluid Velocity (m/s)	0.417
Maximum Fluid Velocity (m/s)	0.625
Reynolds Number	50.505
Maximum Reynolds Number	75.758
Dean Number	5.560

It is aimed to make the users re-think their initial guesses by checking the critical parameters. If there is a parameter with red mark, the user should change the initial guesses until the parameter become satisfying. The facility and fabrication capabilities must be considered while updating the initial guesses.

3.3.3. Database

The database consists of Reynolds number - Focal point tables for different confinement ratio and different Radius of Curvature Ratio values. During the thesis studies, the data base had focus point data for 3 different confinement ratios, 4 different Radius of curvature Ratio and Reynolds number values ranging from 0 to 400.

Table 7 Example of the tables on the database

Reynolds Number – Focusing points				
	Radius of Curvature Ratio			
Reynolds number	**0.0008**	**0.0034**	**0.0083**	**0.0166**
17.323	0.501	0.478	0.429	0.333
25.984	0.501	0.426	0.354	0.316
34.646	0.513	0.522	0.246	0.296
51.969	0.513	0.38	0.33	0.281
70.079	0.513	0.333	0.261	0.278
87.402	0.516	0.243	0.249	0.304
104.724	0.516	0.206	0.293	0.316
122.835	0.513	0.209	0.319	0.333
139.37	0.513	0.22	0.348	0.351
157.48	0.513	0.235	0.365	0.371
174.016	0.504	0.258	0.386	0.4
181.5	0.504	0.276	0.395	0.414
192.913	0.504	0.307	0.409	0.435
209.449	0.154	0.333	0.429	0.467
226.772	0.122	0.359	0.446	0.499
244.094	0.064	0.386	0.464	0.525
262.205	0.067	0.403	0.484	0.554
278.74	0.064	0.426	0.51	0.577
296.063	0.061	0.443	0.528	0.609
314.173	0.061	0.464	0.551	0.629
348.819	0.058	0.499	0.594	0.664
383.465	0.061	0.53	0.623	0.684
418.11	0.058	0.551	0.643	0.716

Particle positions in the articles are normalized between 0 and 1. By presenting the data in a normalized manner, focusing points can be calculated for different spiral microchannels.

It is planned as a future work to transform the database into a platform where data can be added by any user. Adding data will allow the design tool to produce more accurate results.

3.3.4. Interpolations

3.3.4.1. Reynolds Number to Focusing point for Radius of curvature ratio of the user's spiral

The design tool uses a data base gathered from the articles which have a topic of cell separation via spiral microchannels. In the articles many cell separation applications are done via various spiral microchannels with different parameters. It takes the cell focusing positions from the articles and it adapts the results to the user's spiral microchannels. The adaption is done by linear interpolation between two data points for different parameters. The equation of linear interpolation;

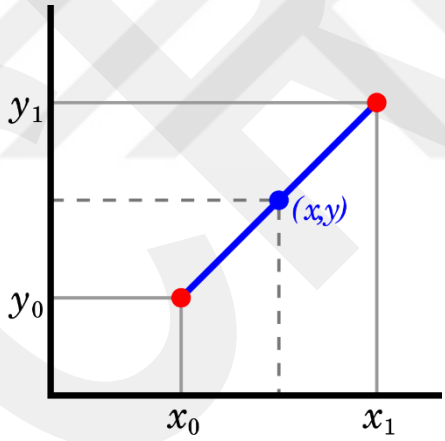

Figure 21 Graphical meaning of the interpolation

$$y = y_0 + (x - x_0)\frac{y_1 - y_0}{x_1 - x_0}$$

In the first step of the calculations, Reynolds number - Focusing point tables are obtained for the radius of curvature ratio of the spiral microchannel of the user. As mentioned before, there are Reynolds number - focal point data for 4 different Radius of curvature ratios in the database. While calculating the radius of curvature ratio, the design tool automatically determines the interval in which the user will perform the interpolation operation. It determines an up and a down value from the user's radius of curvature ratio and uses these points to create Reynolds number - focus point graphs.

Table 8 Example of the first interpolation

Reynolds Number – Focusing points				
	Radius of Curvature Ratio			
Reynolds number	**0.0008**	**0.0034**	**0.0083**	**0.0166**
8.661	0.51	0.443	0.501	0.325
17.323	0.501	0.478	0.429	0.333
25.984	0.501	0.426	0.354	0.316
34.646	0.513	0.522	0.246	0.296
51.969	0.513	0.38	0.33	0.281
70.079	0.513	0.333	0.261	0.278
87.402	0.516	0.243	0.249	0.304
104.724	0.516	0.206	0.293	0.316
122.835	0.513	0.209	0.319	0.333
139.37	0.513	0.22	0.348	0.351
157.48	0.513	0.235	0.365	0.371
174.016	0.504	0.258	0.386	0.4
181.5	0.504	0.276	0.395	0.414
192.913	0.504	0.307	0.409	0.435
209.449	0.154	0.333	0.429	0.467
226.772	0.122	0.359	0.446	0.499
244.094	0.064	0.386	0.464	0.525
262.205	0.067	0.403	0.484	0.554
278.74	0.064	0.426	0.51	0.577
296.063	0.061	0.443	0.528	0.609
314.173	0.061	0.464	0.551	0.629
348.819	0.058	0.499	0.594	0.664
383.465	0.061	0.53	0.623	0.684
418.11	0.058	0.551	0.643	0.716

x0,y0	0.0083	0.501
x1,y1	0.0166	0.325

After this step, the design tool obtains Reynolds Number – Focusing point graphs for three different confinement ratio's available on database.

Table 9 The tables that is going to be obtained after first interpolation

Reynolds number	Focusing Point
8.661	0.420
17.323	0.385
25.984	0.337
34.646	0.269
51.969	0.307
70.079	0.269
87.402	0.274
104.724	0.304
122.835	0.325
139.37	0.349
157.48	0.368
174.016	0.392
181.5	0.404
192.913	0.421
209.449	0.446
226.772	0.470
244.094	0.492
262.205	0.516
278.74	0.541
296.063	0.565
314.173	0.587
348.819	0.626
383.465	0.651
418.11	0.677

3.3.4.2. Reynolds Number to Focusing point for Confinement ratio of the user's cells

As in Radius of curvature ratio, the design tool automatically detects the two closest to the user's confinement ratio value among the 3 confinement ratio values in the database and uses them as data points for interpolation.

As a result of interpolation between these values, Reynolds number - Focusing point graphics are obtained for the particles that the user aims to separate. The focusing point data still presented as normalized manner.

Table 10 Tables that are going to be obtained after the second interpolation

	Confinement Ratio			
	Ref. Particle 1	Ref. Particle 2	User's Particle 1	User's Particle 2
Reynolds Number	**0.066**	**0.0149**	**0.0825**	**0.132**
8.661	0.420	0.432	0.416	0.425
17.323	0.385	0.417	0.374	0.398
25.984	0.337	0.390	0.319	0.359
34.646	0.269	0.381	0.233	0.316
51.969	0.307	0.368	0.288	0.333
70.079	0.269	0.346	0.244	0.301
87.402	0.274	0.327	0.257	0.296
104.724	0.304	0.294	0.307	0.300
122.835	0.325	0.267	0.344	0.301
139.37	0.349	0.224	0.390	0.297
157.48	0.368	0.179	0.429	0.289
174.016	0.392	0.178	0.462	0.303
181.5	0.404	0.190	0.473	0.315
192.913	0.421	0.194	0.494	0.326
209.449	0.446	0.200	0.526	0.344
226.772	0.470	0.209	0.555	0.361
244.094	0.492	0.223	0.579	0.380
262.205	0.516	0.241	0.605	0.401
278.74	0.541	0.253	0.634	0.421
296.063	0.565	0.266	0.662	0.441
314.173	0.587	0.282	0.685	0.460
348.819	0.626	0.311	0.728	0.495
383.465	0.651	0.334	0.753	0.519
418.11	0.677	0.353	0.781	0.542

3.3.4.3. Focusing points for user's Reynolds number value

After the second interpolation, the design tool obtained a Reynolds number - Focusing point graph for two different cells. The interpolation in this step will be done to calculate the focal points in the Reynolds number that the user wants to work with.

The design tool automatically interpolates between the data points it determines and calculates the normalized focus points of the cells that the user aims to separate.

Table 11 Example of the third interpolation

User's Particle 1	
Reynolds Number	Focusing point
8.661	0.416
17.323	0.374
25.984	0.319
34.646	0.233
51.969	0.288
70.079	0.244
87.402	0.257
104.724	0.307
122.835	0.344
139.370	0.390
157.480	0.429
174.016	0.462
181.500	0.473
192.913	0.494
209.449	0.526
226.772	0.555
244.094	0.579
262.205	0.605
278.740	0.634
296.063	0.662
314.173	0.685
348.819	0.728
383.465	0.753
418.110	0.781

User's Re	121.212	
x0,y0	104.724	0.307
x1,y1	122.835	0.344

Position of the Particle 1
0.341

3.3.5. De-normalization

De-normalization is basically calculating where the cell focusing point, normalized between 0 and 1, will fall within the user's specific microchannel. For this purpose, the normalized value between 0 and 1 is multiplied by the width of the user's microchannel.

Table 12 De-normalization process

Normalized cell positions		De-normalized cell positions		Difference (um)
Cell #1	Cell #2	Cell #1	Cell #2	
0.341	0.303	85.241	75.711	9.531

3.3.6. Iterations

In addition to calculating cell focus points, the design tool also checks whether this distance can be achieved by asking the user the distance between the cells you are targeting. If the distance between the targeted cells can be obtained with the current parameters, it marks the result with green color, and if the targeted distance cannot be achieved, it marks the result with red color for the user.

When the distance between the targeted cells cannot be obtained, it iterates at different Reynolds numbers in order to give feedback to the user, checks whether the targeted distance can be achieved or not, and tells the user which Reynolds number to work for the targeted distance.

Since the Reynolds number is related to the Dean number, it also calculates the Dean number corresponding to that Reynolds number as well as the distance calculations between the particles and checks whether the condition of 10< Dean number <25, which is one of the first conditions, is met. Reynolds number values satisfying the intercellular distance and Dean number conditions are marked with green color. Values that do not comply with the conditions are marked with red color.

With this feature of the Design tool, it is aimed to be a more interactive and feedback tool.

Table 13 Iteration and feedback process

	Particle 1	Particle 2	Non-normalized		Difference (μm)	Dean Number
Reynolds Number	Focusing point	Focusing point	Focusing point	Focusing point		
8.661	0.416	0.425	104	106	2	0.95
17.323	0.374	0.398	94	100	6	1.91
25.984	0.319	0.359	80	90	10	2.86
34.646	0.233	0.316	58	79	21	3.81
51.969	0.288	0.333	72	83	11	5.72
70.079	0.244	0.301	61	75	14	7.72
87.402	0.257	0.296	64	74	10	9.62
104.724	0.307	0.300	77	75	2	11.53
122.835	0.344	0.301	86	75	11	13.52
139.370	0.390	0.297	97	74	23	15.34
157.480	0.429	0.289	107	72	35	17.34
174.016	0.462	0.303	115	76	40	19.16
181.500	0.473	0.315	118	79	39	19.98
192.913	0.494	0.326	124	82	42	21.24
209.449	0.526	0.344	132	86	46	23.06
226.772	0.555	0.361	139	90	48	24.97
244.094	0.579	0.380	145	95	50	26.87
262.205	0.605	0.401	151	100	51	28.87
278.740	0.634	0.421	158	105	53	30.69
296.063	0.662	0.441	165	110	55	32.60
314.173	0.685	0.460	171	115	56	34.59
348.819	0.728	0.495	182	124	58	38.40
383.465	0.753	0.519	188	130	59	42.22
418.110	0.781	0.542	195	135	60	46.03

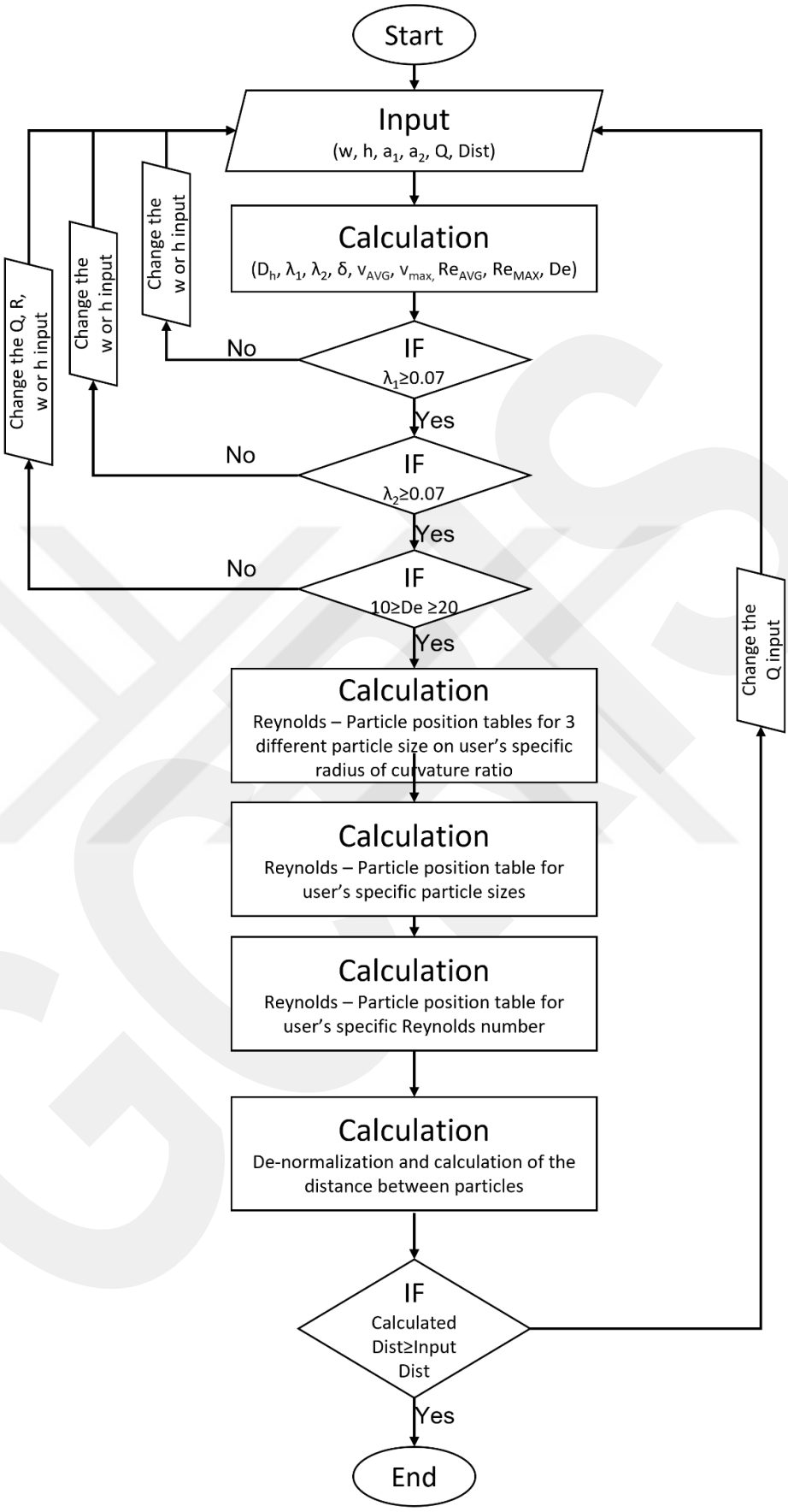

Figure 22 Algorithm flow chart of the design tool

CHAPTER 4

EXPERIMENTAL VALIDATION OF THE TOOL

4.1. MICROCHIP FABRICATION

Microchips with different channel sizes and radius of curvature ratios should be produced. Within the scope of this study, three different types of chips were fabricated, and several experiments were carried out with these chips.

The microchip comprises a silicon and a glass part. Both parts are subjected to different operations.

4.1.1. Operations for Silicon Wafer

Fabrication starts with a cleaning process; Piranha and buffered hydrofluoric acid solution (BHF) cleanings were done to the silicon wafer. Piranha is mixture of H_2SO_4, H_2O_2 and water. The purpose of the process is to get rid of any contaminants. The photolithography step follows this step. Photolithography can be defined as obtaining patterns that are going to be protected from etching agents. In the photolithography process, the silicon surface is coated with a chemical called photoresist. UV light is applied to certain parts of the coated surface. These parts are determined with the help of a mask. Photoresist cures under UV light and becomes resistive against etching agents. The third step is the etching step. The etching step is done via Bosch (Deep Reactive Ion Etching) method. In the process, C_4F_8 and SF_6 reactive gasses are used for passivation and etching operations. Firstly, C_4F_8 gas is applied to the wafer, generating passivation on the active and photoresist-coated surfaces. Afterward, the surfaces are bombarded with fluorine ions to remove passivation layer on the desired locations. The purpose of the second gas application is to obtain linearity on the channel walls. Fluorine ions only remove passivation on horizontal surfaces. Passivation on vertical surfaces such as channel walls is preserved.

Finally, non-passivated and non-photoresist coated surfaces were etched via fluorine radicals. Fluorine radicals etch the silicon and the microchannels generated with these three operations. To increase the linearity, repeating frequency of these steps must be increased too.

On the fourth step, the remaining photoresist is lifted off with O_2 plasma. After step three and step four, the patterns were obtained of the active surface of the silicon wafer, but the surface might still contain contaminants, and any contaminant might cancel the whole MEMS fabrication process, which is why a piranha, nitric acid, and BHF cleaning conducted again as step six. Since the microfluidic channels and the fluid inlet and outlet ports are on the silicon wafer, an additional etching process is required. The important thing about the second etching process is to protect the patterns etched on the first etching process. For that purpose, a thermal SiO_2 film with 0.5 µm thickness was coated on the reverse side of the silicon wafer. Likewise, the sixth step of the fabrication is a 1 µm thick SiO2 film coated on the surface with patterns via the PECVD method. Afterward, steps two, three, and four are repeated to obtain the fluid inlet and outlet ports. We now have a silicon wafer with microchannels and fluid inlet and outlet ports. However, the thickness of the SiO2 film coated on the front and back surface of the silicon wafer is different. In order to eliminate this thickness difference, the whole silicon dioxide film is etched with BHF, and the whole wafer is coated with 0.5 µm silicon dioxide by thermal oxide coating method.

4.1.2. Anodic Bonding

In the fabrication process, the anodic bonding method was used to bond the silicon and glass surfaces together and provide sealing. In the anodic bonding method, an electrical field is applied to the silicon and glass wafers, and the operation is carried out in an environment with a high temperature. Owing to this method, two wafers are bonded to each other without an intermediate layer.

Microchip fabrication generally consists of processes applied to silicon wafers. The glass wafer must not contain contaminants. With this motivation, piranha cleaning is done to the glass wafer, and the wafer is made ready for anodic bonding.

4.2. EXPERIMENTAL WORK

The purpose of the experiments is to pass the microbeads in the channel under different flow rates and to take the recordings while the beads passing through the microchannel. The recordings are analyzed to find the focusing positions of the microbeads. In the experiments, the volumetric flow and microbead size in the microchannel are changed. Other parameters are kept constant. An experiment setup was designed with this motivation (figure).

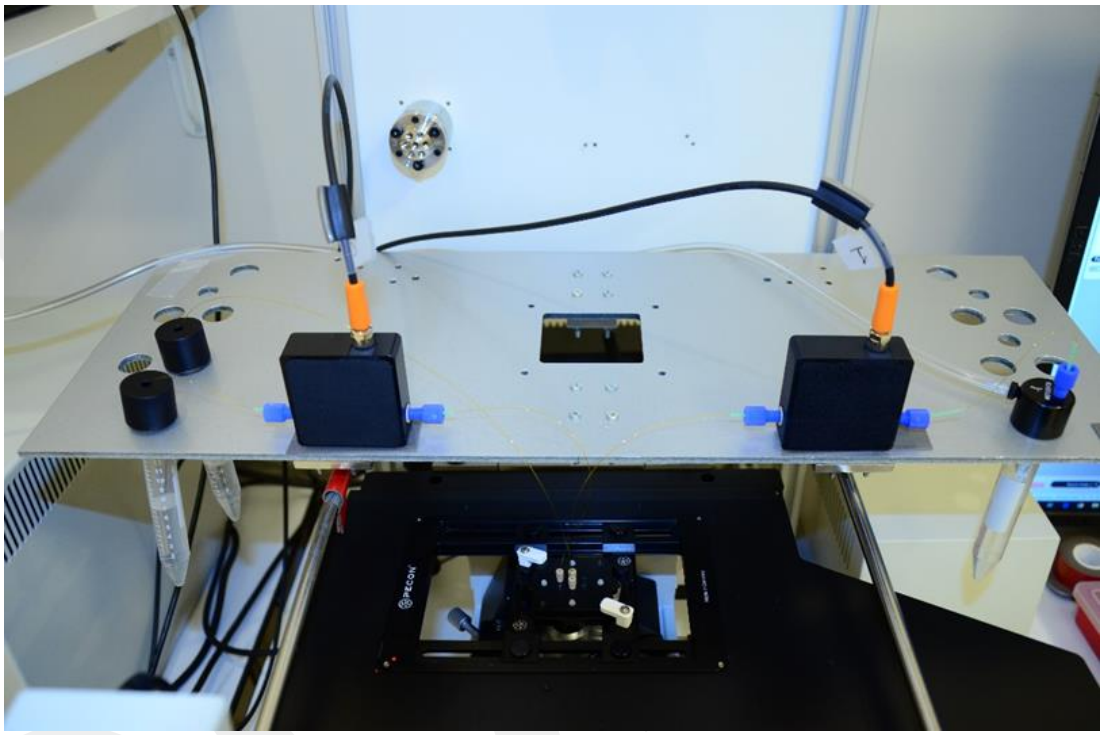

Figure 23 Experimental setup

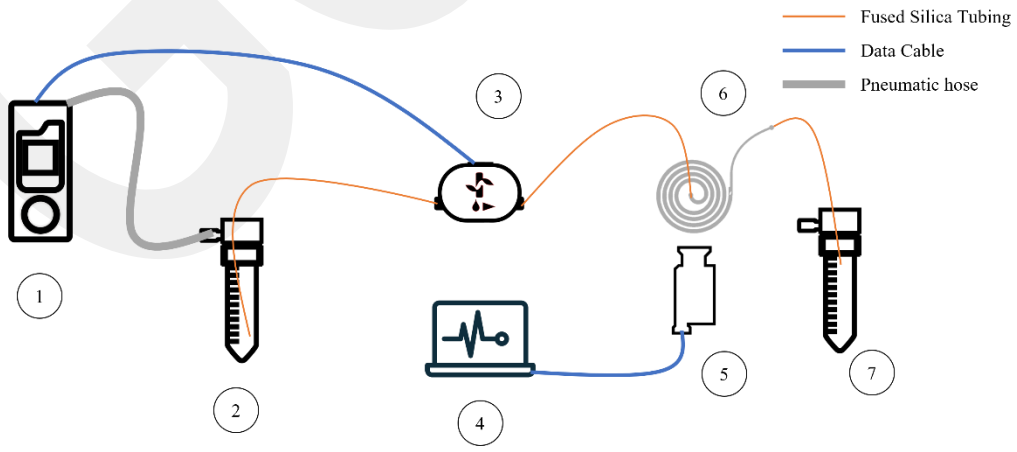

Figure 24 Schema of the experimental setup

4.2.1. Experimental Equipment

1. Pressure Controller

The pressure controller regulates the pressure coming from a source and applies it into a pressure tubing. FlowEZ 7000 (Fluigent, Germany) pressure controller was used to pressurize the inlet reservoir and apply fluid into the system. The pressure controller can be either controlled via computer, or it can work standalone.

2. Inlet Centrifuge Tube

15 mL centrifuge tubes (Isolab, Germany) are used as a fluid reservoir. One piece of inlet tube contains the sample, and one piece of outlet tube was used to collect the sample passed through the system.

3. Flow Sensor

In the experiments, a thermal flow sensor (Flow Unit XL, Fluigent, Germany) was used to measure the flow rate inside of the system. It applies heat to the fluid, and it measures the change in temperature of the fluid. By measuring the temperature difference, it calculates the flow rate. It is very advantageous to use electronic equipment with the same brand. The most important advantage is the fully automatic communication between them. By connecting them, desired flow rate value can be directly applied to the system, which was the method used in the experiments.

4. Computer

The computer is used to observe and record the flow in the microchannel with the help of a microscope, to see if there is a situation that may disrupt the flow, and to observe the operation parameters such as volumetric flow in the channel in real-time.

5. Microscope

The particle positions were observed in the experiments via inverted fluorescent microscope (DMI8, Leica, Germany). DMI8 has four different fluorescent filters that enable us to observe blue, green, and red colored fluorescent microbeads. Microscope image

6. Microchip

The microchip is the main element in which the operation takes place. All elements other than the microchip are auxiliary elements for the microchip to perform its function. The microchip is made of silicon-glass material with a spiral microchannel, fabricated with MEMS technology.

7. Outlet Centrifuge Tube

This setup is designed so that the flow in the system can be observed continuously, and real-time and different flow rates can be easily applied. Three different flow rate values were tried for each microchip and these values were determined with the design tool.

8. Tube Adapter

The tube adapter is the tool that fits to the centrifuge tubes and connects the microfluidic fittings to the centrifuge tube. The adapter's primary purpose is to isolate the centrifuge tube and enable pressure application to the centrifuge tube. Therefore, the thread type of the adapter and the tube should match perfectly. Also, to obtain isolation, there should be a seal between the adapter and the tubes. In experiments, Elveflow's centrifuge tube adapters were used.

9. Tubing

Fused silica tubing (Postnova, USA) pieces with 250 um inner diameter and 360 um outer diameter are used to fluid transportation between system components. The primary material of the fused silica tubing is glass, and the outer side of the glass is coated with PET to reduce the fragility.

10. Pneumatic hose

A polyurethane pneumatic tubing with 4x6 measurements was used to supply pressurized nitrogen to the pressure controller.

11. Fittings

- 1/8" - 28 UNC to 4 mm fitting (Elveflow, France)

Fitting was used to connecting the pneumatic tubing and centrifuge tube adapter.

- 1/8" - 28 UNC fitting (Elveflow, France)

Fitting was used to connecting the Fused silica tubing and centrifuge tube adapter. It is also used to connect the Fused silica tubing and flow sensor.

- 6-32 UNC fitting (Postnova, USA)

Fitting was used to making fluidic connections to a microfluidic chip.

12. Ferrules

- 10° angled conical ferrule (Elveflow, France) with 1.6mm inner diameter

The ferrule is fully compatible with 1/8" UNC fitting, which is used to seal the connection on the tube adapter and flow sensor; it prevents fluid leakage.

- Nanoport ferrule (Postnova, USA)

The ferrule was used to seal the connection between the chip and fused silica tubing.

13. Sleeve

A micro-tight sleeve (Postnova, USA) was used to adapt the fused silica tubing to the 10° angled conical ferrule. It has an inner diameter of 0.39 mm and an outer diameter of 0.63. The material of FEP.

14. Chip holder

Chip Holder is the component that enables us to make fluidic connections to the microchip. It has threaded holes at positions aligned with the fluid inlet and outlet ports at the microchip. The thread type on the holes is 6-32 UNC, which matches the thread type of the 6-32 UNC fitting. The chip holder comprises two parts—the cap part and the window part. The fluidic connection holes are placed on the cap part. On the other hand, the window part contains a rectangular hole for the observation of the microchip. The hole must be big enough that the whole spiral can be observed.

4.2.2. Sample Preparation

In the experiments, due to the ethical regulations, instead of live cells, 10 and 16 µm sized fluorescent microbeads (Brand, Country) were used to mimic white blood cells (WBC) and circulating tumor cells (CTC). The microbeads were suspended in 10 ml of deionized water with nearly 2 million total beads. 3 drops were taken from each product and suspended into filtered deionized water. Afterward, deionized water was added until the concentration of the sample was reduced to 2×10^6 per milliliter. The concentration of the samples was measured via an automated cell and bead counter (TC20®, Bio-Rad, USA).

In order to prevent agglomerations and adhesion of the beads, it is required to add a surfactant (Tween®20, Sigma-Aldrich, Germany). The volume of the surfactant is related to the volume of the sample. As a result, 10 mL samples with 2x 10^6 pieces per milliliter 10 and 20 µm beads were obtained.

4.2.3. Pre-operation (Conditioning) Step

The pre-operation process is the process of getting the chip ready for cell or bead samples. The high roughness surfaces obtained in MEMS productions are very suitable for the adhesion of cells and microbeads. There are three primary purposes of the pre-operation process:

1. Sterilization of the chip and other components

One of the consequential purposes of liquid biopsy is to enable personalized medicine. To enable personalized medicine, the patient's cancer cells should be collected without damaging them, and these cells must be progenitive. Contamination of the bacteria, virus or other single-cell living beings may corrupt the product. By applying ethanol, sterilization of the chip was done.

2. Getting rid of air bubbles

Thermo-polymers generally have hydrophobic characteristics, so there is a possibility of air bubble formation in the microchannels. Air bubble formations causing changes in the hydraulic resistance and lead cells to illogical destinations. Application of the ethanol also cleans the system from air bubbles.

3. Prevention of cell or bead adhesion

To prevent the adhesion, we can either change the adhesive nature of the cells or beads or coat the chip's surface. There are a few surfactant options to coat the surfaces on the market, like Tween® 20 (Sigma Aldrich, Germany) and random graft co-polymer with a poly(L-lysine) backbone and poly (ethylene glycol) side-chains (PLL-g-PEG Polymer – SuSoS, Switzerland).

1 mg of the powder form of the PLL-g-PEG, which stored at -20 °C temperature, resolved into 10 ml of deionized water and incubated inside of the microchannel for 30 minutes.

It should not be exposed to light and heat. It should be stored at +4 °C temperature after the PEG- deionized water mixture prepared.

The conditioning process begins with passing ethanol through the channel. The purpose of passing ethanol is to prevent the formation of air bubbles in the channel and to sterilize the channel. Afterwards, deionized water is passed through the channel until there is no ethanol in the channel. The time required for this is 2 minutes. Afterwards, the channel walls are coated with PLL-g-PEG surfactant. To obtain an efficient coating,

In PLL-g-PEG treatment, 1000 mbar pressure was applied to the system until the deionized water inside the system was replaced with PLL-g-PEG solution, which required 45 seconds. Afterward, the pressure was reduced to 12.5 mbar, and the flow was stopped after 30 minutes. The coating requires a zero-flow rate in the system. The

head loss and elevation differences cause a negative flow rate. 12.5 mbar pressure is applied to the system to balance the backpressure caused by head loss in the system.

4.2.4. Operation Step

Three different flow rates were tried on three different microchips with different parameters, and these three flow rate values were specific for each microchip. The specifications and the parameters of the microchips that have been used in the experiments were given below.

During the operation, two critical points were checked in real-time.

1. Dirt

Dirt is one of the biggest problems in microfluidic applications because even a tiny particle can affect the flow if it is stuck at any portion of the channel. This would change the streamlines and possibly alter the particle positions.

2. The volumetric flow rate

The flow rate can change due to dirtiness, blockage, malfunction of hardware, or leakage. The flow rate can either increase or decrease as a result of these problems. An increase or decrease in the flow rate means that the system is not working with preferred parameters. The system can tolerate an increase or decrease of 50 microliters per minute in the flow rate in the channel. However, for changes larger than this value, repeating the experiment or the possible results of this problem should be evaluated.

4.2.5. Post-operation (Cleaning) Step

At the end of each experiment, the system should be cleaned from cell or bead residue. A potassium-hydroxide based cleaning solution named ICF (Guava Instrument Cleaning Fluid, ICF, Merck, Germany) was used to clean the system to get rid of these contaminants. ICF is incubated in the system for 15 minutes for thoroughly cleaning. After ICF is passed through the microchannel, the ICF in the system should be washed with deionized water. For an efficient washing, 2 ml of deionized water is given into the system with a pressure of 1000 mbar. Filtered isopropanol is passed through the washed system and the system is dried with pressurized nitrogen gas. The pressure applied during the isopropanol application and drying is 1000 mbar.

4.2.6. Data Analysis

Obtained experimental images need to be analyzed. This analysis includes image processing the recording video obtained with the microscope. the recordings were taken while the microbeads pass through the channel. The recordings were taken via Bandicam software.

For image processing, ImageJ software was used. ImageJ is an open-source tool for image processing applications [34]. The screenshots of the recordings were captured by VLC Video Player with a 1000 fps of capture rate.

Taken screenshots are opened in ImageJ software as an image sequence and the average of the pixel brightness of all screenshots is taken. When these screenshots are averaged, they become a single photograph, which shows us where the fluorescently glowing microbeads pass through in the microchannel. In order to find the focused position of the microbeads, distance measurement is made again with ImageJ software. For this, we need to define the distance of which we know the length in ImageJ and enter this distance. For this, the channel width is selected. By scaling the distance of the channel width, the distance of the starting and ending positions of the microbeads to the inner wall is calculated. In this way, it is calculated at which position a microbead of a certain size will be focused in the channel under certain parameters.

CHAPTER 5

RESULTS AND DISCUSSION

5.1. NUMERICAL MODEL AND DESIGN TOOL COMPARISON

Within the scope of the thesis, a previously produced spiral channel was modeled and numerical CFD analyzes were made. At the same time, these channel dimensions were entered into the Design tool, the focal points of the cells were calculated, and experimental studies were carried out with microbeads and the results were compared. The CFD simulation were done a PC with an Intel 7th generation Processor that has CPU Maximum Turbo frequency of 4.1 GHz and 32 GB RAM capacity.

CFD analyzes were run with different mesh qualities and it was investigated what kind of changes different mesh qualities cause in the results.

The table below presents the number of elements of different mesh qualities and the time taken for simulations with these element numbers.

Table 14 Mesh quality, number of mesh and required time for analysis table for CFD simulations

Mesh Quality	Number of Mesh	Required time for analysis (hours)
Extremely coarse	11218	~16
Coarser	48584	~19
Coarse	148287	~23
Normal	271074	~26
Fine	752169	~45

The simulations were run under laminar flow conditions and the flow rate in the channel was determined as 1.0 ml/min. Under laminar flow conditions, particles with a size of 10 micrometers were introduced into the channel from the inlet side and

their focused positions on the outlet side were tried to be determined. The effects of drag force and lift force on the particles are defined. Since secondary flow occurs spontaneously in curved channels, the effects of Dean forces can be seen automatically. It has been proved by plotting the flow streamlines in the cross-sectional plane that the secondary flow occurs.

In the CFD analysis, in simulations with low mesh number, it was observed that the particles adhered to the inner wall after advancing a little in the channel and moved adjacent to the inner wall in the rest of the channel. It was observed that the distance traveled by the particles before adhering to the inner wall increased as the mesh number increased.

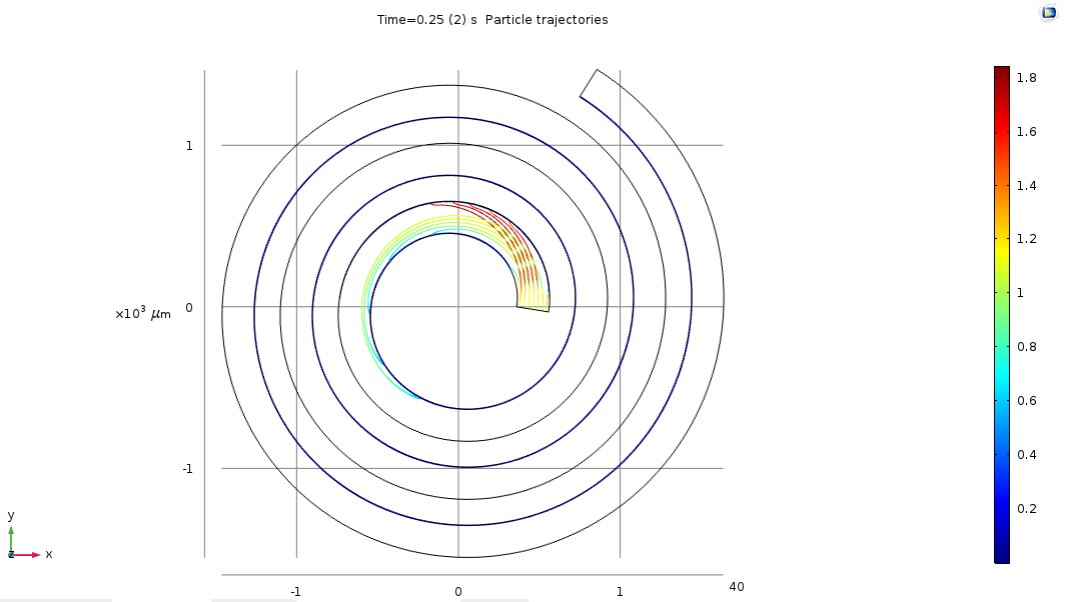

Figure 25 Particle trajectories for the simulations with coarser mesh quality

In Coarser mesh quality, the particles adhere to the inner wall before the first round of the spiral is finished and thus complete the rest of the channel.

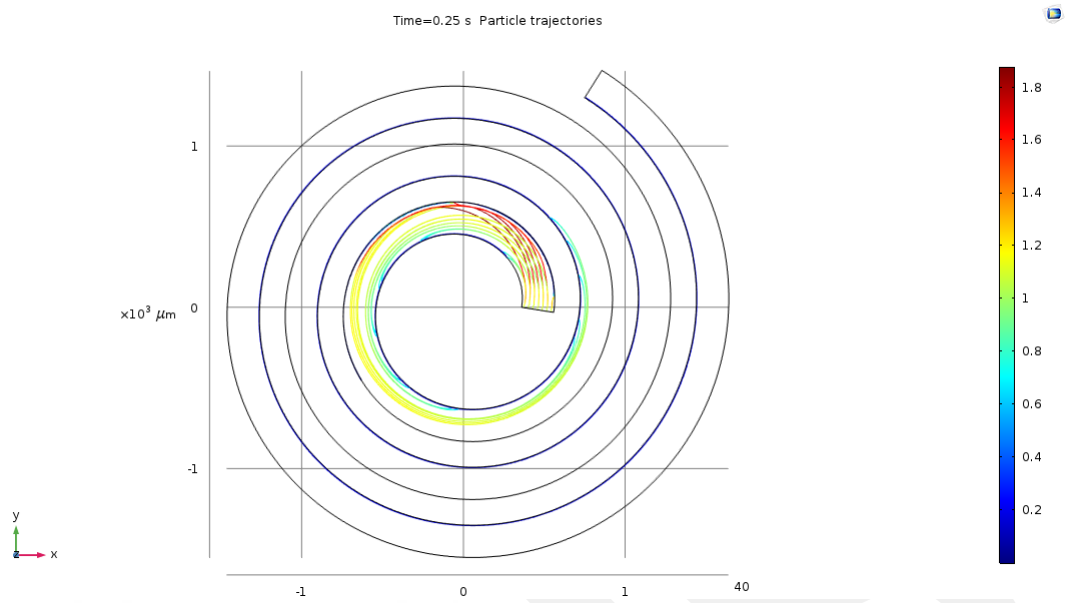

Figure 26 Particle trajectories for the simulations with normal mesh quality

In normal mesh quality, it was observed that the particles adhered to the inner wall immediately after completing the first round of the spiral.

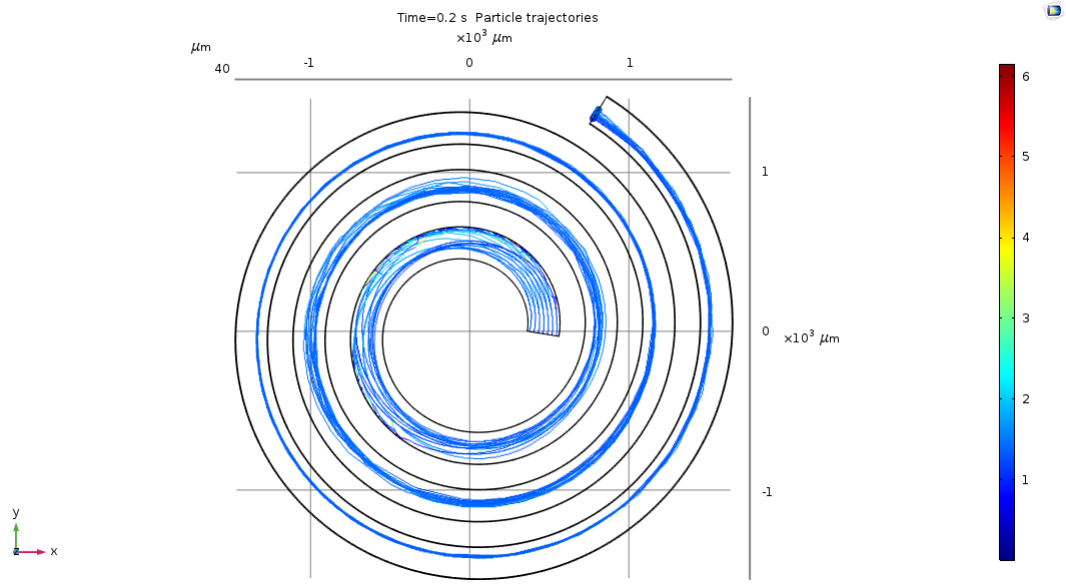

Figure 27 Particle trajectories for the simulations with fine mesh quality

In the simulations with fine mesh quality, particles adhering to the inner wall were not observed. As expected, the particles are focused in a certain area after moving a little in the channel.

Even with fine mesh quality, unreasonable particle movements are observed in the starting regions of the channel. This shows us that even Fine mesh quality may not be enough. A fine mesh quality simulation takes approximately 45 hours to complete.

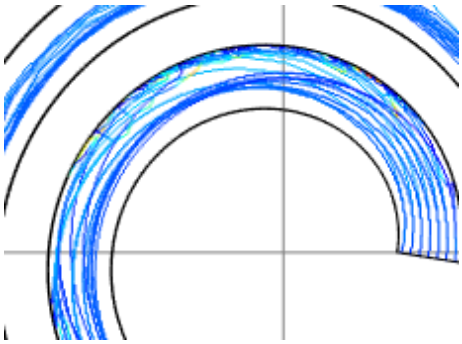

Figure 28 Illogical particle trajectories in fine mesh quality simulation

Design tool and CFD analysis have advantages and disadvantages compared to each other. The design tool eliminates the need for a high-end computer required for CFD analysis, significantly reduces the analysis time, and allows the user to test multiple spiral microchannels in a short time. In addition, it is an important feature for users to give feedback to the user and advise on the operating conditions. Besides, using the design tool, it is not possible to get the answer whether the cells can be collected from the desired output or not. The design tool only gives information about the locations where the cells will focus. By modeling the outputs in CFD simulations, it can be observed whether the cells can be directed to the desired output or not. At the same time, it is not possible with the design tool to observe the effects of different geometric structures to be added into the channel on cell separation.

5.2. FINE MESH SIMULATION, EXPERIMENTAL AND DESIGN TOOL COMPARISON

Due to the limitations in the production methods of microbeads, it is impossible to produce exactly the desired size, but it can be produced with a certain margin of error. According to the information provided by the Manufacturer, the average size of microbeads sold as "10 µm" is 10.2 micrometers. The smallest microbead size is 9.2 micrometers and the largest microbead size is 11.2 micrometers. Therefore, there are microbeads of variable size in the sample prepared for experiments, and microbeads of different sizes are focused at different points. Given this fact, it would be unreasonable to give a single value when comparing the experimental result and the results obtained with the design tool. With this motivation, particle sizes were determined as the smallest microbead sizes in the design tool and results were obtained according to these dimensions. The same is true for CFD simulations.

Table 15 Cell focusing position comparison between CFD simulation and Design tool

	Cell distance to inner wall (um)		
Size of the cell (um)	**CFD Simulation**	**Design Tool**	**Experiment**
9.20	90	72	79
11.20	38	67	58

When the analysis and test results with the same operating parameters were compared, the results given in the table below were obtained. When the results were evaluated, it was seen that the results obtained with the 3 methods were like each other. Here, it was seen that the results obtained with the design tool had a narrower interval than the results obtained with other methods.

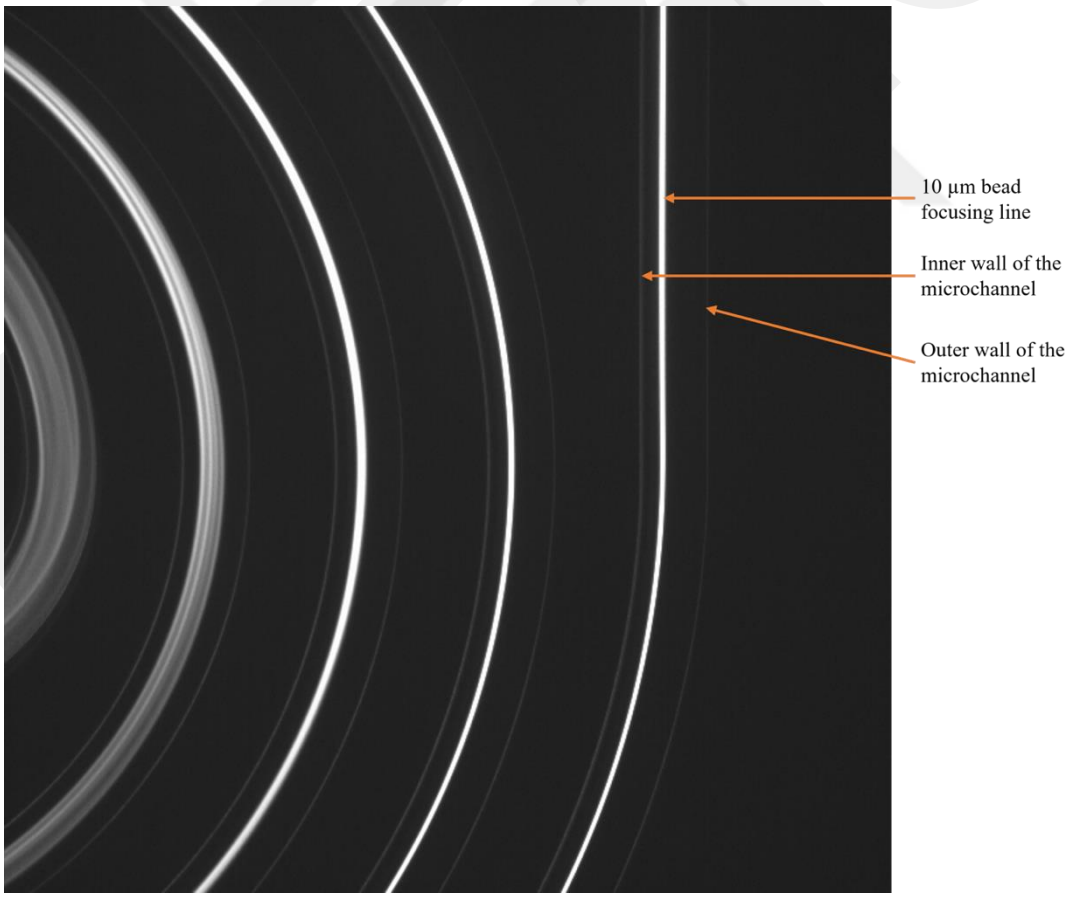

Figure 29 Experimental image of cell focusing inside of the spiral microchannel

5.3. EXPERIMENT AND DESIGN TOOL RESULTS

The size variations encountered in microbead sizes apply not only to 10 micrometer microbeads but also to 20 micrometer beads. Microbeads sold in 20 micrometer size consist of the smallest 18.4 micrometer and the largest 21.6 micrometer microbeads, so the results were calculated based on these sizes in the analyzes.

Considering the variations in size, we see that the particles are focused as a distribution within the microchannel.

The results obtained from the design tool and the experiments and the locations within the microchannel to which these results correspond are presented below.

Table 16 Focusing positions that is provided by design tool and obtained from experiments for 1.0 ml/min flow rate

Flow Rate (ml/min)	1.0	
Reynolds Number	83.3	
	Bead distance to the inner wall (um)	
Bead size (um)	Design tool	Experiment
9.2	92	103
10.8	90	89
18.4	67	72
21.6	72	59

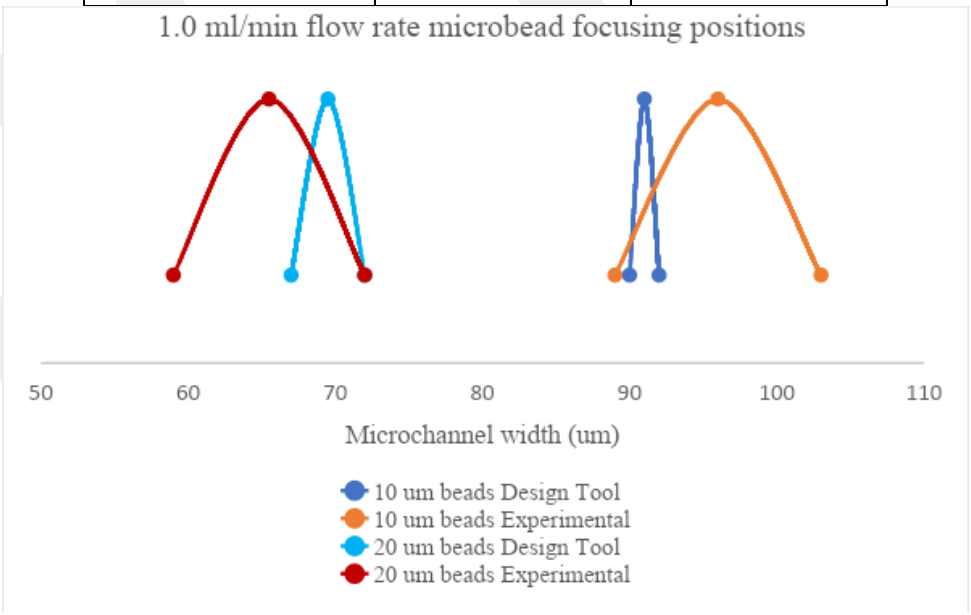

Figure 30 Microbead migrating distributions provided by Design tool and obtained by experiments for 1.0 ml/min

Table 17 Focusing positions that is provided by design tool and obtained from experiments for 1.5 ml/min flow rate

Flow Rate (ml/min)	1.5	
Reynolds Number	125	
	Bead distance to the inner wall (um)	
Bead size (um)	Design tool	Experiment
9.2	105	126
10.8	101	108
18.4	79	82
21.6	70	66

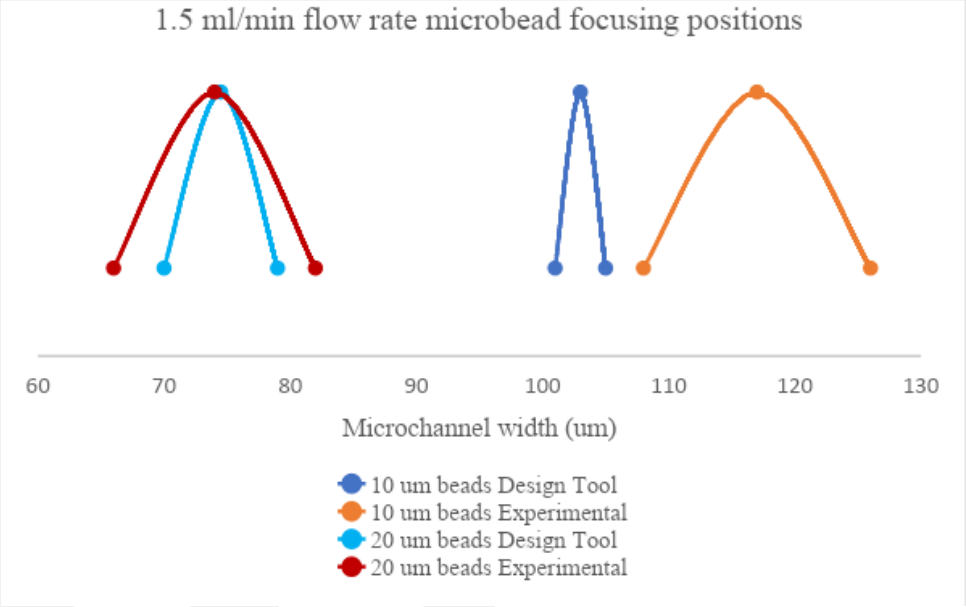

Figure 31 Microbead migrating distributions provided by Design tool and obtained by experiments for 1.5 ml/min

Table 18 Focusing positions that is provided by design tool and obtained from experiments for 2.0 ml/min flow rate

Flow Rate (ml/min)	2.0	
Reynolds Number	167	
	Bead distance to the inner wall (um)	
Bead size (um)	Design tool	Experiment
9.2	112	129
10.8	107	101
18.4	88	86
21.6	78	74

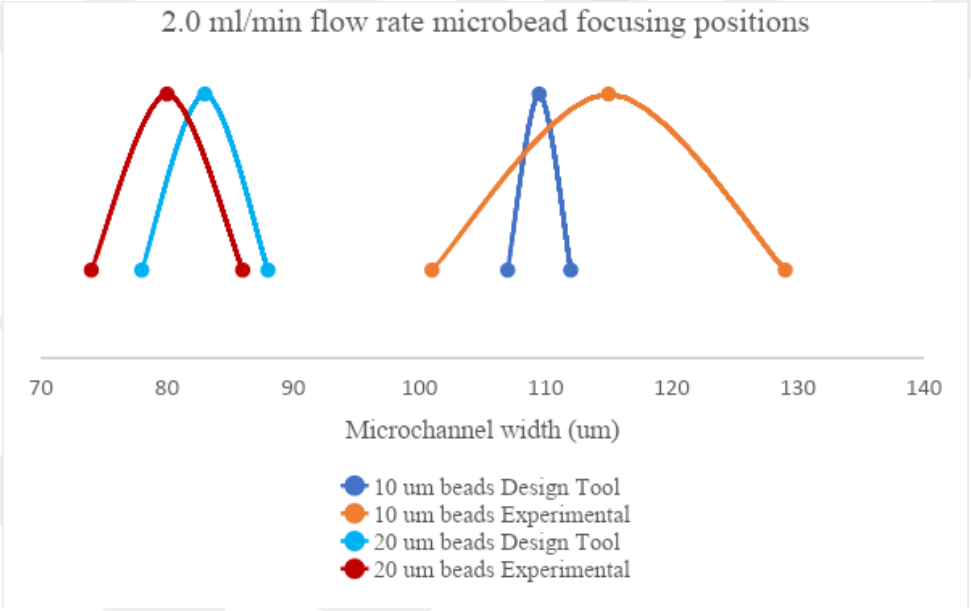

Figure 32 Microbead migrating distributions provided by Design tool and obtained by experiments for 2.0 ml/min

When the results were evaluated, it was seen that the thickness of the focusing line was less in the results given by the Design tool. This may be due to the fact that the size variation of the microbeads is actually wider. As a result of the investigation of the microbead sizes with an automatic cell counter, it was observed that the microbead sizes generally matched the manufacturer's data, but the presence of a certain amount of irregular microbead sizes was also observed. The number of irregular microbeads is considerably less than the number of regular microbeads, but

since an analysis on brightness was made, irregular microbeads affect the experimental results.

The reason for the general differences in the results is the use of linear interpolation during data adaptation. It is assumed that the line between the two data points is linear during the calculations. However, when the data in the database was plotted, it was seen that the value between the two points was not linear. Therefore, it is thought that a secondary polynomial or a third order polynomial solution will give more accurate results instead of linear interpolation. The graphs below are presented to prove the correctness of this idea.

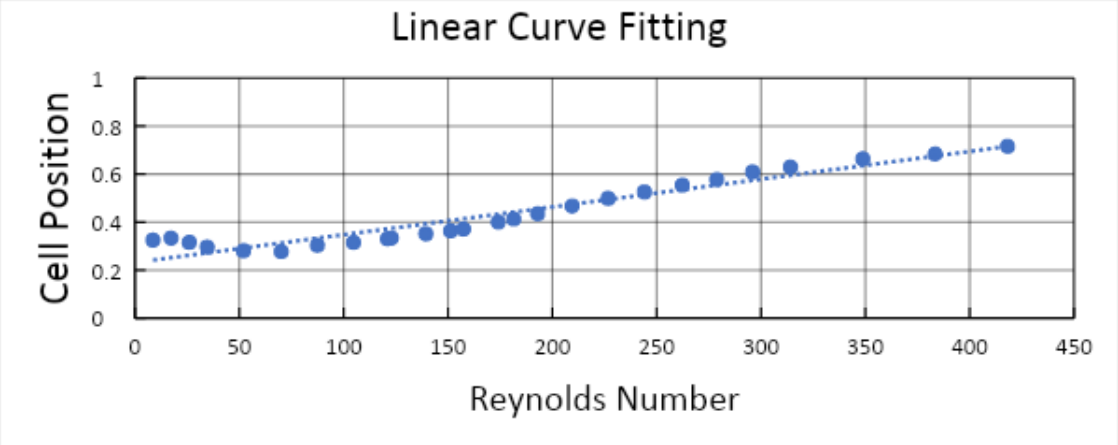

Figure 33 R^2 value of linear curve fitting

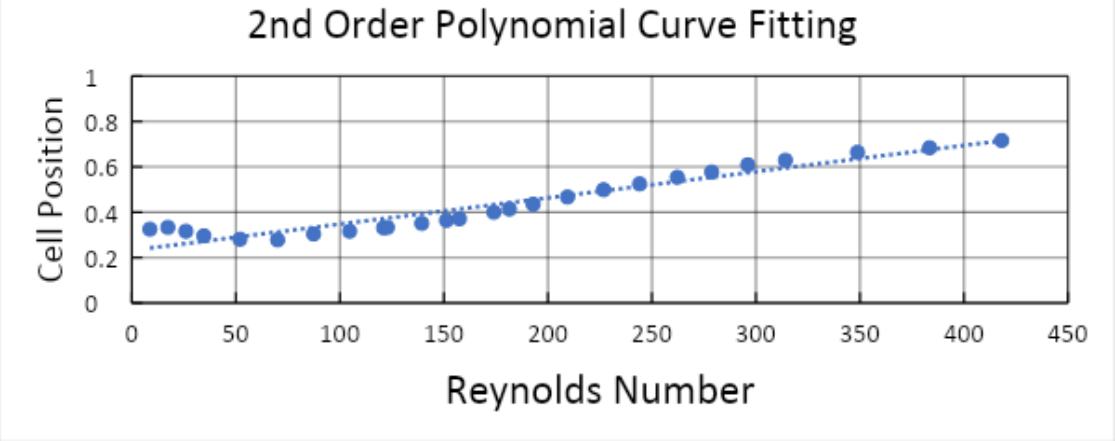

Figure 34 R^2 value of 2nd order polynomial curve fitting

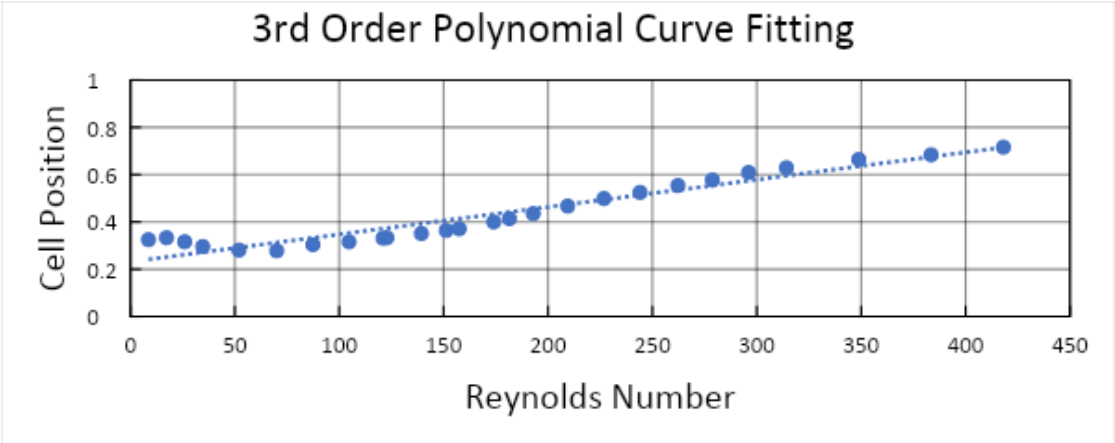

Figure 35 R^2 value of 3rd order polynomial curve fitting

REFERENCES

[1] "Richard Feynman 'Tiny Machines' Nanotechnology Lecture - aka 'There's Plenty of Room at the Bottom' - YouTube." https://www.youtube.com/watch?v=4eRCygdW--c&t=174s (accessed Nov. 01, 2021).

[2] Nam-Trung Nguyen, S. Wereley, and S. A. M. Shaegh, *Fundamentals and Applications of Microfluidics*, vol. 110, no. 9. 2019.

[3] R. M. Guijt and A. Manz, "Miniaturised total chemical-analysis systems (MTAS) that periodically convert chemical into electronic information," *Sensors Actuators, B Chem.*, vol. 273, pp. 1334–1345, 2018, doi: 10.1016/j.snb.2018.06.054.

[4] J. V. Frangioni, "New technologies for human cancer imaging," *J. Clin. Oncol.*, vol. 26, no. 24, pp. 4012–4021, 2008, doi: 10.1200/JCO.2007.14.3065.

[5] J. L. Pool, "Magnetic resonance imaging," *Biomed. Instrum. Technol.*, vol. 36, no. 5, pp. 341–346, 2002, doi: 10.2345/0899-8205(2002)36[341:TFOMRI]2.0.CO;2.

[6] A. Norman, "On the origin of cancer foci," *Cancer*, vol. 5, no. 3, pp. 581–582, 1952, doi: 10.1002/1097-0142(195205)5:3<581::AID-CNCR2820050319>3.0.CO;2-Q.

[7] K. Pantel and C. Alix-Panabières, "Liquid biopsy and minimal residual disease — latest advances and implications for cure," *Nat. Rev. Clin. Oncol.*, vol. 16, no. 7, pp. 409–424, 2019, doi: 10.1038/s41571-019-0187-3.

[8] M. Mischel, F. Rougé, I. Lamprecht, C. Aubert, and G. Prota, "Dielectrophoresis of malignant human melanocytes," *Arch. Dermatol. Res.*, vol. 275, no. 3, pp. 141–143, 1983, doi: 10.1007/BF00510042.

[9] Y. Huang, X. B. Wang, F. F. Becker, and P. R. C. Gascoyne, “Introducing dielectrophoresis as a new force field for field-flow fractionation,” *Biophys. J.*, vol. 73, no. 2, pp. 1118–1129, 1997, doi: 10.1016/S0006-3495(97)78144-X.

[10] H. Shafiee, J. L. Caldwell, M. B. Sano, and R. V. Davalos, “Contactless dielectrophoresis: A new technique for cell manipulation,” *Biomed. Microdevices*, vol. 11, no. 5, pp. 997–1006, 2009, doi: 10.1007/s10544-009-9317-5.

[11] J. Y. Chan *et al.*, “Dielectrophoresis-based microfluidic platforms for cancer diagnostics,” *Biomicrofluidics*, vol. 12, no. 1, 2018, doi: 10.1063/1.5010158.

[12] A. P., M. C., N. M., L. H., and L. T., “Microfluidic, label-free enrichment of prostate cancer cells in blood based on acoustophoresis,” *Anal. Chem.*, vol. 84, no. 18, pp. 7954–7962, 2012, [Online]. Available: http://www.embase.com/search/results?subaction=viewrecord&from=export&id=L365663101%5Cnhttp://dx.doi.org/10.1021/ac301723s%5Cnhttp://sfx.library.uu.nl/utrecht?sid=EMBASE&issn=00032700&id=doi:10.1021%2Fac301723s&atitle=Microfluidic%2C+label-free+enrichment.

[13] M. C. Zalis *et al.*, “Label-free concentration of viable neurons, hESCs and cancer cells by means of acoustophoresis,” *Integr. Biol. (United Kingdom)*, vol. 8, no. 3, pp. 332–340, 2016, doi: 10.1039/c5ib00288e.

[14] M. Dao *et al.*, “Acoustic separation of circulating tumor cells,” *Proc. Natl. Acad. Sci. U. S. A.*, vol. 112, no. 16, pp. 4970–4975, 2015, doi: 10.1073/pnas.1504484112.

[15] L. Luo and Y. He, “Magnetically driven microfluidics for isolation of circulating tumor cells,” *Cancer Med.*, vol. 9, no. 12, pp. 4207–4231, 2020, doi: 10.1002/cam4.3077.

[16] K. H. Han, A. Han, and A. B. Frazier, “Microsystems for isolation and electrophysiological analysis of breast cancer cells from blood,” *Biosens. Bioelectron.*, vol. 21, no. 10, pp. 1907–1914, 2006, doi: 10.1016/j.bios.2006.01.024.

[17] W. Zhao *et al.*, “Label-Free and Continuous-Flow Ferrohydrodynamic Separation of HeLa Cells and Blood Cells in Biocompatible Ferrofluids,” *Adv.*

Funct. Mater., vol. 26, no. 22, pp. 3990–3998, 2016, doi: 10.1002/adfm.201503838.

[18] H. Chen, Z. Zhang, H. Liu, Z. Zhang, C. Lin, and B. Wang, "Hybrid magnetic and deformability based isolation of circulating tumor cells using microfluidics," *AIP Adv.*, vol. 9, no. 2, 2019, doi: 10.1063/1.5081849.

[19] N. Pamme, "Magnetism and microfluidics," *Lab Chip*, vol. 6, no. 1, pp. 24–38, 2006, doi: 10.1039/b513005k.

[20] O. Philippova, A. Barabanova, V. Molchanov, and A. Khokhlov, "Magnetic polymer beads: Recent trends and developments in synthetic design and applications," *Eur. Polym. J.*, vol. 47, no. 4, pp. 542–559, 2011, doi: 10.1016/j.eurpolymj.2010.11.006.

[21] Y. Yu, Y. Yang, J. Ding, S. Meng, C. Li, and X. Yin, "Design of a Biocompatible and Ratiometric Fluorescent probe for the Capture, Detection, Release, and Reculture of Rare Number CTCs," *Anal. Chem.*, vol. 90, no. 22, pp. 13290–13298, 2018, doi: 10.1021/acs.analchem.8b02625.

[22] H. Zhang and K. K. Liu, "Optical tweezers for single cells," *J. R. Soc. Interface*, vol. 5, no. 24, pp. 671–690, 2008, doi: 10.1098/rsif.2008.0052.

[23] S. G. P. Id *et al.*, "A microfluidic-based filtration system to enrich for bone marrow disseminated tumor cells from breast cancer patients," 2021, doi: 10.1371/journal.pone.0246139.

[24] E. Oosterbroek, *Modeling , Design and Realization of Microfluidic Components (tesis doctoral)*. 1996.

[25] J. Zhang *et al.*, "Fundamentals and applications of inertial microfluidics: A review," *Lab Chip*, vol. 16, no. 1, pp. 10–34, 2016, doi: 10.1039/c5lc01159k.

[26] Y. Gao, "Inertial migration of particles in microchannel flows Yanfeng Gao To cite this version : HAL Id : tel-01630993," no. June, 2019.

[27] D. Di Carlo, "Inertial microfluidics," *Lab Chip*, vol. 9, no. 21, pp. 3038–3046, 2009, doi: 10.1039/b912547g.

[28] J. M. Martel and M. Toner, "Inertial focusing dynamics in spiral microchannels," *Phys. Fluids*, vol. 24, no. 3, pp. 1–13, 2012, doi: 10.1063/1.3681228.

[29] N. Nivedita, P. Ligrani, and I. Papautsky, “Dean Flow Dynamics in Low-Aspect Ratio Spiral Microchannels,” *Sci. Rep.*, vol. 7, no. February, pp. 1–10, 2017, doi: 10.1038/srep44072.

[30] D. Di Carlo, D. Irimia, R. G. Tompkins, and M. Toner, “Continuous inertial focusing, ordering, and separation of particles in microchannels,” *Proc. Natl. Acad. Sci.*, vol. 104, no. 48, pp. 18892–18897, 2007, doi: 10.1073/pnas.0704958104.

[31] M. E. Warkiani *et al.*, “Slanted spiral microfluidics for the ultra-fast, label-free isolation of circulating tumor cells,” *Lab Chip*, vol. 14, no. 1, pp. 128–137, 2014, doi: 10.1039/c3lc50617g.

[32] G. Özkayar *et al.*, “A novel microfluidic method utilizing a hydrofoil structure to improve circulating tumor cell enrichment: Design and analytical validation,” *Micromachines*, vol. 11, no. 11, pp. 1–17, 2020, doi: 10.3390/mi11110981.

[33] J. M. Martel and M. Toner, “Particle focusing in curved microfluidic channels,” *Sci. Rep.*, vol. 3, pp. 1–8, 2013, doi: 10.1038/srep03340.

[34] “ImageJ.” https://imagej.nih.gov/ij/index.html (accessed Nov. 01, 2021).